$\frac{37}{7-28-80}$

UCID- 18732

Beam Deflection into a Quadrant by a Positionally Stationary Magnetic Bending System

Arthur C. Paul
Lawrence Berkeley Laboratory
Berkeley, California

V. Kelvin Neil
Lawrence Livermore National Laboratory
Livermore, California

MASTER

June 20, 1980

Lawrence Livermore Laboratory

Beam Deflection into a Quadrant by a Positionally Stationary Magnetic Bending System*

Arthur C. Paul,
Lawrence Berkeley Laboratory
Berkeley, California

V. Kelvin Neil
Lawrence Livermore National Laboratory
Livermore, California

ABSTRACT

A system of postionally stationary magnets is analyzed for the continuously variable deflection of a 50 MeV electron beam. The system is composed of a collection of horizontal and vertical bending magnets, quadrupoles, and a final deflection magnet that is conical in shape and capable of deflections of plus or minus 50 degrees simultaneously in both horizonal and vertical planes. Throughout the system the beam is assumed to be focused by its own magnetic self-field, the electric self-field being neutralized by background ions. The motion of the beam in the externally applied magnetic fields may then be considered as single particle motion. The system of bending magnets and quadrupoles pre-conditions the beam by introducing the proper displacements and angles at the entrance to the final deflection magnet for momentum deviations up to plus or minus one percent. The displacements and angles are determined by the chromaticity of the final deflection magnet and are a function of the bending angles in the two planes. The total system is then doubly achromatic in both planes. The pre-conditioning magnets are of standard accelerator beam transport design while the conical deflection magnet is of a design fashioned from a television deflection coil scaled up by about a factor of 10 in size.

*Lawrence Livermore National Laboratory is operated by the University of California for the Department of Energy under Contract No. W-7405-Eng-48.

This work is performed by LLNL for the Department of Defense under DARPA (DOD) ARPA Order 3718, Amendment #12, monitored by NSWC under Contract No. N60921-80-WR-W0188.

Introduction

The system shown in Fig. 1 is considered in detail in this report. The designation of the sections of the system and the individual magnets shown in the figure will be used throughout this work. Linear particle optics are employed to first order in the momentum deviation. It is assumed that gas focusing of the beam prior to entrance into the system results in a beam with negligible transverse dimensions and thus the motion in the externally applied magnetic fields is that of a single particle. The dispersion of the final deflection magnet (hereafter referred to as the "snout" magnet) is a known function of the bending angles α_h and α_v in the horizontal and vertical planes respectively. The beam passing through the pre-conditioning magnets is given values of x, x', y, y' at the entrance to the snout according to the momentum deviation. These quantities are individually selected by four "tuning knobs" on the preconditioner. The values selected are those that make the total system doubly achromatic in both planes.

We emphasize that only linear theory is employed in this paper and that certainly second order effects must be considered in future work. Furthermore in the mathematical model of the snout that we use, motion in the two transverse planes is not coupled, while in a practical snout they will generally be coupled. This coupling in a real snout does not alter our conclusions that a preconditioner can be designed to provide the required angles and displacements at the snout entrance since the coupling will merely give different values from those we consider. The values required by a practical snout as well as second order effects may dictate a preconditioner that is more complex than the rather simple arrangement considered in this work.

We shall refer to the preconditioner and the snout as the deflection system. The system consists of five sections, four of which make up the preconditioner and the fifth is the snout magnet. Each section of the preconditioner consists of a single magnet or an array of magnets and drift spaces. We describe briefly the matrix formalism of conventional beam transport theory that is used in this report[1], and outline the principle employed in the design of the preconditioner.

A particle with momentum p that enters a section at the proper position and at the proper angle we call the reference particle, and we call its trajectory the reference trajectory. The momentum p is that for which the entire system has been tuned. Other particle trajectories will have deviations from the reference trajectory, both in position and angle. These deviations are x, y, x', and y', where x and y are the distances from the reference trajectory in the two transverse planes and the prime indicates the slope relative to the reference trajectory. Particles may also have a momentum deviation dp and and a path length deviation ds. Thus each trajectory is characterized by a six-dimensional vector. The vector V^+ exiting the section is related to the vector V^- entering the section by the matrix equation,

$$V^+ = RV^-. \tag{1.1}$$

The matrix R is the transport matrix of the section and is the product of the matrices of the magnets and drift spaces that make up the section. The transport matrix of the system is the product of the matrices of the sections that make up the system. The elements of the 6 X 6 matrix of a section are determined by the configuration of magnetic fields and drift spaces throughout the section.

The path length deviation does not enter our calculations, therefore we are dealing with 5 X 5 matrices. We will, however, retain the conventional notation and write the matrix equation in the form

$$\begin{bmatrix} x \\ x' \\ y \\ y' \\ \frac{dp}{p} \end{bmatrix}^{+} = \begin{bmatrix} R_{11} & R_{12} & R_{13} & R_{14} & R_{16} \\ R_{21} & R_{22} & R_{23} & R_{24} & R_{26} \\ R_{31} & R_{32} & R_{33} & R_{34} & R_{36} \\ R_{41} & R_{42} & R_{43} & R_{44} & R_{46} \\ 0 & 0 & 0 & 0 & 1 \end{bmatrix} \begin{bmatrix} x \\ x' \\ y \\ y' \\ \frac{dp}{p} \end{bmatrix}^{-} \qquad (1.2)$$

The matrix elements R_{16}, R_{26}, R_{36}, and R_{46} are the dispersion elements of the matrix. The quantities $R_{16}dp/p$ and $R_{36}dp/p$ are the positional dispersion and the quantities $R_{26}dp/p$ and $R_{46}dp/p$ are the angular dispersion. To avoid confusion, we say that if both the positional and angular dispersion are zero in one plane the section is doubly achromatic in that plane. If the section bends the beam in one transverse plane only, it is conventional that the top two rows of the matrix transform the displacement and angle in the bend plane and the third and fourth rows transform the displacement and angle in the non-bend plane. We will not follow that convention consistently in this work.

In general the matrix of the snout will have all the elements indicated in Eq. (1.2). These elements will be functions of the deflection angles α_h and α_v, and we assume that the matrix elements can be found by computation and or measurement to the degree of accuracy required. In this work, the assumption of decoupled planes allows us to take $M_{13} = M_{14} = M_{23} = M_{24} = M_{31} = M_{32} = M_{41} = M_{42} = 0$. The trajectory of a particle exiting the snout is represented by the vector V_s^+ and we have

$$V_s^+ = R_s V_s^-, \tag{1.3}$$

in which V_s^- represents the trajectory entering the snout. The + and − superscript convention will be retained throughout this work. for all deflection angles α_h and α_v the desired form of V_s^+ is

$$V_s^+ = (0, 0, 0, 0, dp/p). \tag{1.4}$$

We multiply Eq. (1.3) on the left by the inverse of R_s and set $R_s^{-1}R_s = I$, the identity matrix, and obtain,

$$V_s^- = R_s^{-1}V_s^+. \tag{1.5}$$

The physical meaning of Eqs. (1.4) and (1.5) is graphically illustrated in Fig. (2). The vector V_s^- in general has all five components non-zero. For any values of α_h and α_v, V_s^- gives the values of x, x', y, and y' as a function of dp/p that must be provided at the entrance to the snout by the preconditioner in order for V_s^+ to have the form given by Eq. (1.4). Within the linear theory employed in this work, x, x', y, and y' are linear functions of dp/p and it is therefore possible to preconditon the beam with four sections.

We call the first section of the preconditioner the horizontal corrector (HC). The section consists of three bending magnets and two drift spaces.

The trajectories of all particles entering the HC are represented by the same vector, V_{hc}^-, which is identical to V_s^+ and given Eq. (1.4). The HC provides a horizontal displacement only, so that $V_{hc}^+ = (x_1, 0, 0, 0, dp/p)$. The value of x_1 is that necessary to pass through the rest of the preconditioner and arrive at the snout entrance with the desired vector. We let R_{hc} be the matrix of the HC. The second section is the horizontal quadrupole section (focusing in the horizontal plane), which we call QH. It turns out that two quadrupoles and a drift space are needed in this section for some vertical deflection angles, but for this discussion we simply employ the matrix R_{qh} for this section. The QH provides a value of x' but does not contribute to y and y', so that $V_{qh}^+ = (x_2, x'_2, 0, 0, dp/p)$. The values x_2 and x'_2 are not those required at the snout entrance because the next two sections are focusing and defocusing in the horizontal plane. The values are those required to pass through the remaining two sections and arrive at the snout with the desired vector.

The third section is the vertical corrector VC. It is identical to the horizontal corrector except it is rotated 90 degrees. The VC provides a displacement y and new values of x and x', so that $V_{vc}^+ = (x_3, x'_3, y_3, 0, dp/p)$. The fourth section of the preconditioner is the vertical quadrupole section (focusing in the vertical plane), QV. This section provides the desired value of y' and changes the values of x, x', and y to the desired values at the entrance to the snout. Since the initial vector $V_{hc}^- = V_s^+$, the condition on the matrices of the five sections of the system is

$$R_s R_{qv} R_{vc} R_{gh} R_{hc} = I,$$

or,

$$R_{qv} R_{vc} R_{qh} R_{hc} = R_s^{-1}.$$

In the following treatment the problem is actually worked backwards from the snout, using the inverse matrices of the sections. For given α_h and α_v the desired values of x, x' y, and y' are determined from the knowledge of R_s^{-1}. The QV section is set to make y' = 0 (going backwards) and this setting determines values of x_3, x'_3, and y_3. The VC section is set to make y = 0 and determine values of x_2 and x'_2. The QH section is set to make x' = 0 and determine the value of x_1 that must be provided by the HC section.

2. Snout Magnet

Figure 3 is a photogragh of a yoke magnet that directs the electron beam onto the shadow screen of a television picture tube. Such a magnet, which is capable of simultaneous large angle deflections in both horizontal and vertical directions is the principal component of the deflection system we are considering. The aberrations inherent in the magnet are assumed to be known functions of the bending angles α_h and α_v.

A. Physical Model of the Deflection Magnet.

To gain some insight into the chromatic aberrations of the snout, we have investigated the coil configuration shown in Fig. 4. The origin of a rectangular coordinate system is located 10 cm below the narrow end of the cone, and the z axis lies along the axis of the cone. The angle of the cone is 70 degrees and the height is 0.9 m. For deflection in one plane (x as shown) two nine turn coils are wound on the surface of the cone. The choice of nine turns is made for convenience. In practice the coil would have many more turns. In a cross-section normal to the axis, the conductors are placed to approximate a surface current distribution proportional to cos θ. All of the turns close in the θ direction at the ends of the cone. For deflection in the y direction an identical pair of nine turn coils is placed on the surface, but rotated 90 degrees about the z axis. This second pair of coils is shown in the figure, separated from of horizontal pair for clarity. These two sets of coils approximate a crossed dipole magnetic field configuration.

The magnetic field from these coils has been computed[2]. Figure 5 shows the contours of constant B_y in the plane $y = 0$ for a current of 10 kA in the horizontal deflection coils. We note that this field configuration bears no resemblance to the field in conventional bending magnets in accelerators and beam transport systems. In conventional bending magnets the magnetic field is uniform or has a specified radial gradient. The field in the cone magnet resembles more the fringing field at the edge of a conventional magnet, where it is sometimes useful, but more often a nuisance.

The trajectories of 50 MeV electrons in the $y = 0$ plane have been computed[3] for various currents in the horizontal deflection coils, and are shown in Fig. 6. The angle of bend and the ampere turns/coil necessary to obtain that angle are given. A 7 kA current correspondes to 6.3×10^4 ampere-turns in each coil of the pair. We note that the trajectory exiting at 56 degrees passed through the surface of the cone, indicating that to achieve bending angles greater than about 50 degrees the coils would not be placed on the surface of a cone, but rather be shaped similarly to the television yoke in Fig. 3. In the television industry, the yoke is referred to as a saddle coil[4]. Figure 7 shows the ampere-turns required to achieve a given bending angle.

If the deflection is in the horizontal plane only, the matrix elements R_{36} and R_{46} in Eq. (1.2) are zero and the elements R_{16} and R_{26} are non-zero. The units of R_{16} and R_{26} are meters/fraction (cm/percent) and rad/fraction (10mrad/percent) respectively. These dispersion elements are plotted vs α_h in Fig. 8. The values were obtained by integrating over path lengths of 1 meter and 1.5 meters, and we see that there is considerable difference. For small angles of deflection the difference between the curves for one meter path length and 1.5 meter path length corresponds to the effect of drift on the matrix elements. That is, these trajectories are clear of the magnetic field after 1 meter and for the remaining one-half meter we have $x = x_o + Lx'_o$, where L is the drift length, while $x' = x'_o$. For large angles the trajectories lie near the coils and are not clear of the field after 1 meter. The "exit" of the conical snout is a bit nebulous, however we will employ an analytic model of the snout in the following treatment.

For a given dp/p the locus of points in the $x - x'$ plane found by varying α forms a curve that we will call the dispersion curve. It is the parametric curve (with α the parameter) of R_{26} vs R_{16}, and it is shown in Fig. 9 for a path lengths of 1 m and 1.5 m. For linear optics employed here, the curve is to be interpreted in the following manner: A particle with momentum p will exit from the cone at the origin in the $x - x'$ plane, independent of the angle α. A particle with momentum 1.01p will exit at some point on the curve, the location of the point being determined by the angle α. For the same angle α, particles with momentum between p and 1.01p will exit at a point lying on a straight line linking the origin with the point on the curve, the distance from the origin being porportional to dp, as shown in Fig. 9 for $\alpha = 50.6^{\circ}$ and 1.5 m path length. For negative dp the straight line extends through the origin to the reflected point on the curve.

B. Analytic Model of the Deflection Magnet.

In order to avoid the necessity of numerical integration of trajectories in the magnetic field of the cone, we will use an analytic model for the snout matrix. We consider a conventional bending magnet with a dispersion curve matching that of the cone in the $y = 0$ plane to a rather good approximation. The idealized magnet has uniform magnetic field in the bend plane. Furthermore, the exit edge of the model magnet is shaped so that the angle between the particle trajectory at exit and the normal to the edge is equal to one half the bending angle and provides vertical focusing. The geometry is shown in Fig. 10. The value of L for the model in chosen so that the angular and positional dispersion matrix elements R_{16} and R_{26} match that of the physical model, Fig. 8, for $\alpha = 42.7^\circ$. The transport matrix for the model magnet in the bend plane is

$$R_3 = \begin{bmatrix} \cos\alpha & L\cos\alpha/2 & L\sin\alpha/2 \\ \dfrac{-2\sin\alpha/2\tan\alpha/2}{L} & 1 & 2\tan\alpha/2 \\ 0 & 0 & 1 \end{bmatrix} \qquad (2.1)$$

Figure 9 shows the dispersion curve for this matrix for L = 1.2165 m. We see that the curve approximates that found for the cone by integrating trajectories over 1 m path length. The curve of the analytic model with L = 1.2165 m followed by a 0.5 m drift approximates the curve found for the cone by integrating trajectories over 1.5 m path length.

The matrix for the model magnet in the non-bend plane is

$$R_{sx} = \begin{pmatrix} 1 & \dfrac{L\,\alpha}{2\sin\alpha/2} & 0 \\ -\dfrac{2}{L}\sin\dfrac{\alpha}{2}\tan\dfrac{\alpha}{2} & 1-\alpha\tan\dfrac{\alpha}{2} & 0 \\ 0 & 0 & 1 \end{pmatrix}. \qquad (2.2)$$

We do not employ this matrix in our work. Because of the assumption of uncoupled motion, both the x and y planes are transformed by the bend plane matrix in Eq. (2.1).

3. Horizontal and Vertical Correctors

The HC and VC sections are identical arrays of three dipole bending magnets, the VC being rotated 90 degrees about the z axis with respect to the HC. In discussing these arrays we take the x plane to be the bending plane as it is in the HC section. These sections are fashioned from the dispersionless three magnets array shown in Fig. 11. The presence of the symmetry plane S - S guarantees that the array is doubly achromatic. Particles with different momenta follow different trajectories through the array, but all trajectories exit the array on the same beam line as at entry. We call trajectories with this property colinear.

Introducing an asymmetry into the array produces a beam with positional dispersion at the exit. If the magnets are properly tuned, the reference particle with momentum p follows a colinear trajectory as shown in Fig. 12. As defined in the figure, the bending angles θ_1, θ_2, and θ_3 of the reference particle in the three bending magnets must satisfy two conditions. First, in order for the reference particle to exit at the proper angle, we have

$$\theta_2 = \theta_1 + \theta_3. \tag{3.1}$$

Second, in order for the reference particle to exit at the proper position, we have

$$L_1 \tan(\theta_1/2) + S_1 \tan\theta_1 - L_2 \tan(\theta_3 - \theta_1)/2$$
$$- S_2 \tan\theta_3 - L_3 \tan(\theta_3/2) = 0. \tag{3.2}$$

In this expression L_1, L_2, L_3, S_1 and S_2 are the magnet lengths and separations as shown in Fig. 12. With these conditions, a value of θ_1 determines values of θ_2 and θ_3. The values of θ_2 and θ_3 that satisfy Eqs. (3.1 and 3.2) are plotted vs. θ_1 in Fig. 13 for $L_1 = L_2 = L_3 = 0.5$ m, $S_1 = 1$ m and $S_2 = 0.5$ m. These dimensions are arbitrarily chosen, and we will use them throughout this work.

Particles with momentum p + dp will exit the array with a displacement in the bend plane proportional to dp, as shown qualitatively in Fig. 14 for θ_1 both positive and negative. The array results in positional dispersion but no angular dispersion. For $\theta_1 > 0$ a positive momentum deviation produces a negative displacement, while for $\theta_1 < 0$ a positive momentum deviation produces a positive displacement. The convention of positive or negative displacement is based on the sign of the positional dispersion matrix element, R_{16}. This dispersion element is plotted vs. θ_1 in Fig. 15, and is found to be well approximated by the relation

$$R_{16} = -a\,\theta_1\, e^{b\theta_1}, \tag{3.3}$$

with R_{16} in cm/%, θ_1 in degrees, $a = 4.78 \times 10^{-4}$, and $b = 0.1014$. In the following we refer to θ_1 in the HC as θ_h, and θ_1 in the VC as θ_v.

Focusing in the non-bend plane is provided by the fringing fields at magnet 1 exit, magnet 2 entrance and exit, and magnet 3 entrance because the tragectories are not normal to the magnet edge at these locations. In the bend plane, edges are defocusing but the bends are focusing so that the net effect is that the array provides no net focusing. The transport matrix elements of the sections for the non-bend plane are plotted in Fig. 16, and the elements for the bend plane are plotted in Fig. 17. In these figures we have used the convention that the top two rows of the matrix transforms the bend plane. Since the array is a drift space for motion in the bend plane. $R_{11} = R_{22} = 1$ and R_{12} is the effective path length through the array as a function of θ_1.

The matrix elements in Eq. (1.2) that couple the x and y motion are zero throughout the preconditioner. These elements are R_{13}, R_{14}, R_{23}, R_{24}, R_{31}, R_{32}, R_{41} and R_{42}.

4. Dispersive Preconditioning

With the analytic model, Eq. (2.1), for the transport matrix of the snout, and the matrix elements of the HC and VC sections displayed in Figs. 15, 16, and 17, we may write the matrices and inverse matrices of the five section of the deflection system.

We now adopt the convention that the first two rows of our matrices transform motion in the horizontal (x) plane and the second two rows transform motion in the vertical (y) plane. Since the vector $V_s^+ = (0, 0, 0, 0, dp/p)$, we need only the last column of the inverse matrix R_s^{-1}. We generate the matrix R_s^{-1} from the matrix R_s given by Eq. (2.1) and find that the vector V_s^- at the entrance to the snout is given by

$$V_s^- = \left[L \sin \frac{\alpha_h}{2} \; , -\sin \alpha_h, \; L \sin \; \frac{\alpha_v}{2} \; , -\sin \alpha_v, \; 1 \right] \quad dp/p. \qquad (4.1)$$

There is a vertically focusing quadrupole, QV, between the VC and the snout as shown in Fig. 18. We use the thin lens approximation for both the QV and the QH sections, with equal drift spaces of length D on either side. The inverse matrix R_{qv}^{-1} is given by

$$R_{qv}^{-1} = \begin{bmatrix} 1 + D/f & -(2D + D^2/f) & 0 & 0 & 0 \\ -1/f & 1 + D/f & 0 & 0 & 0 \\ 0 & 0 & 1 - D/f & -2D + D^2/f & 0 \\ 0 & 0 & 1/f & 1 - D/f & 0 \\ 0 & 0 & 0 & 0 & 1 \end{bmatrix} \qquad (4.2)$$

in which f is the focal length of the quadrupole. For the same length drift spaces, the inverse matrix R_{qh}^{-1} for the QH is found from this expression by reversing the sign of f.

In order to display the matrices R_{hc} and R_{vc} for the HC and VC sections respectively, we refer to Figs. 15, 16, and 17. The notation in these figures is such that R_{11}, R_{12}, R_{21}, R_{22}, and R_{16} transform the bend plane and R_{33}, R_{34}, R_{43}, and R_{44} transform the non-bend plane. From the figures we see that $R_{11} = R_{22} = 1$, and $R_{21} = R_{26} = 0$. We define the quantities a, b, c, d, e, and h in terms of the matrix elements in Figs. 16 and 17. This procedure results in some simplified (and hopefully less confusing) notation. We set

$$a = R_{33} \qquad c = R_{43} \qquad e = R_{16}$$
$$\tag{4.3}$$
$$b = R_{34} \qquad d = R_{44} \qquad h = R_{12}.$$

Employing these definitions, we write the matrix R_{hc} for the HC section in the form

$$R_{hc} = \begin{bmatrix} 1 & h & 0 & 0 & e \\ 0 & 1 & 0 & 0 & 0 \\ 0 & 0 & a & b & 0 \\ 0 & 0 & c & d & 0 \\ 0 & 0 & 0 & 0 & 1 \end{bmatrix}. \tag{4.4}$$

The inverse matrix R_{hc}^{-1} is given by

$$R_{hc}^{-1} = \begin{bmatrix} 1 & -h & 0 & 0 & -e \\ 0 & 1 & 0 & 0 & 0 \\ 0 & 0 & d & -b & 0 \\ 0 & 0 & -c & a & 0 \\ 0 & 0 & 0 & 0 & 1 \end{bmatrix}. \tag{4.5}$$

The inverse matrix R_{vc}^{-1} of the VC section is given by

$$R_{vc}^{-1} = \begin{bmatrix} d & -b & 0 & 0 & 0 \\ -c & a & 0 & 0 & 0 \\ & & 1 & -h & -e \\ 0 & 0 & 0 & 1 & 0 \\ 0 & 0 & 0 & 0 & 1 \end{bmatrix}. \tag{4.6}$$

A. Predconditioning in one plane

As an example of how the system is tuned, let us consider the vector V_s^- given by Eq. (4.1). At the entrance to the snout we have

$$y = L \sin \frac{1}{2} \alpha_v \,(dp/p), \tag{4.7a}$$

$$y' = -\sin\alpha_v \,(dp/p) \;. \tag{4.7b}$$

Referring to Eq. (4.2) we see that the condition $y' = 0$ at the exit of the VC determines the focal length, f, of the quadrupole to be

$$f = D - \left(y_s / y'_s\right) \quad . \tag{4.8}$$

The value of y at the exit of the VC determines the setting of the VC. We have

$$y = \left(1 - \frac{D}{f}\right) y_s - \left(2D - \frac{D^2}{f}\right) y'_s$$

with f given by Eq. (4.8). The value of θ_v necessary to achieve this value of y at the exit of the VC is then found from Figs. 15 and 17, or from Eq. (3.3). The focal length of the vertical quadrupole and the value of θ_v are now set to provide doubly achromatic deflection in the vertical plane. But the QV is defocusing in the x plane, and the VC focusing in the x plane. So preconditioning in the x plane is a bit more complicated.

B. A Numerical Example

To demonstrate preconditioning in both transverse planes, we consider deflection angles $\alpha_h = 30^\circ$ and $\alpha_v = 20^\circ$. The momentum deviation is

+1% for this example. The lengths L = 1.2165 m, and D = 0.25 m in both the QV and QH sections, as shown in Fig. 19. The various positions in the system are also designated in the figure. In terms of the notation employed in the introduction, we have $V_s^- = V_2$, $V_{vc}^+ = V_{qv}^- = V_3$, $V_{vc}^- = V_{qh}^+ = V_4$, $V_{qh}^- = V_{hc}^+ = V_5$, and $V_{hc}^- = V_6$. The inverse matrices of the 4 sections of the preconditioner and the vectors at each position are displayed in Table 1. The calculation is performed with x and y in cm and x' and y' in units of 10 mrad.

In Table 1 the vector V_2 is found from Eq. (4.1) with L = 1.2165 m, $\alpha_x = 30^\circ$, and $\alpha_y = 20^\circ$. The inverse matrix R_{qv}^{-1} is given by Eq. (4.2) with D = 0.25 m and f_v determined by Eq. (4.8), which yields $f_v = .8797$ m. To save space, numbers in Table 1 are given to 5 decimal places only, but the calculations were carried out to at least 15 decimal places. The setting of a quadrupole is generally stated as the field gradient times the effective length, which is kG-m/m, or simply kG. The relationship between field strength, focal length, and the magnetic rigidity (B ρ) of the particles is B = (B ρ)/f. For electrons with p = 50.5 MeV/c we have

$$B = 1.68451 \text{ kG-m}/f, \tag{4.10}$$

so that the strength of the vertical quadrupole is −1.9415 kG-m/m for f = .8797 m. By convention the sign of a quadrupole field is positive for horizontal focusing and negative for vertical focusing. In Table 1 the value of y_3' is indicated to be zero, although the numerical calculation yielded a value of 4.8×10^{-7} rad.

The inverse matrix R_{vc}^{-1} is given by Eqs. (4.3) and (4.6). The value of θ_v is chosen to yield e (= R_{16} in Figs. 14 and 16) = .29674. The value of θ_v was not found from the figures or from Eq. (3.3) but was calculated using a special computer code. A value $\theta_v = -29.91808^\circ$ was found to yield the proper value of e (Eq. 4.3). The remaining elements of R_{vc}^{-1} were also calculated with the code.

The inverse matrix R_{qh}^{-1} is found from Eq. (4.2) by reversing the sign of f. The condition $f_h = D - (x_4/x_4')$ yields $f_h = 2.6011$ m, and a corresponding field strength 0.64762 kG-m/m.

The inverse matrix R_{hc}^{-1} is given by Eq. (4.5). The value of $\theta_h = 46.8632^\circ$ was found to yield e = -2.41593. This value as well as the remaining elements of R_{hc}^{-1} was calculated with the code.

5. System Tune for All Deflection Angles

Our deflection system must be capable of aiming the electron beam in any direction. That is, the settings of the four sections of the preconditioner must be reasonable for all combinations α_h and α_v, as shown in Fig. 20. The system shown in Fig. 19 is inadequate in that values of α_v near 4° cannot be accomodated. Figure 21 shows the angles θ_h and θ_v and the quadrupole settings Q_v and Q_h (in kG-m/m) as functions of α_v for dp/p = 1% and $\alpha_h = 10^\circ$, 20°, 30° and 40°. The settings Q_v and θ_v are independent of α_h, and the setting Q_h varies by less than 1% for $0 < |\alpha_h| < 50^\circ$. We see that there is a singularity in the setting Q_h and an abrupt change in the sign of θ_h at $\alpha_v \simeq 4^\circ$.

The singularity in the setting Q_h can be understood from the horizontal dispersion curve at the entrance to the VC. In Fig. 22 the values of x' and x at this position are plotted for dp/p = 1%, $\alpha_h = 30^\circ$ and $-50^\circ < \alpha_v < 50^\circ$. We see that the value of x passes through zero at $\alpha_v \approx 4^\circ$, and therefore the QH section can have no effect upon particle trajectories. For $\alpha_v < 4^o$ the sign of both Q_h and θ_h are reversed.

Physically the singularity arises because of the focusing properties of the VC section in the horizontal plane. The VC is focusing in the horizontal plane and for $\alpha_v > 4^o$ there is a momentum focus (i.e., a point where x = 0 regardless of the value of dp) within the VC. As the vertical deflection is reduced with the associated reduction in vertical correction, this momentum focus in the x plane shifts toward the entrance to the VC. For $\alpha_v < 4^o$ the momentum focus lies upstream of the VC. The position of the momentum focus for different values of α_v is shown qualitatively in Fig. 23, which displays the trajectories in the X plane of particles with momentum p and $p \pm dp$.

The tuning singularity can be removed by the addition of a second horizontally focusing quadrupole, with setting Q_x, to the QH section as shown in Figs. 1 and 23. The QH section with 2 quadrupoles can no doubt be operated in several ways in order to provide the required values of x and x' at the entrance to the VC. One mode of operation is to maintain the same setting of Q_h for all α_v less than some value, and obtain the required values of x and x' at the entrance to the VC with the setting of Q_x. For smaller values of α_v (and θ_v) the horizontal focus lies upstream of the quadrupole Q_h. The clamped setting of Q_h is sufficient to insure that the momentum focus lies between Q_h and Q_x, and elimnates the necessity of θ_h changing sign at $\alpha = 4^o$.

We consider the geometry shown in Fig. 23, with two thin lens quadrupoles separated by a distance L_x. There is a drift distance D between the entrance to the VC and the quadrupole Q_h and between the quadrupole Q_x and the exit of the HC. Since y and y' are zero throughout the HC and the QH sections, we need consider only the elements 11, 12, 21, and 22 of the inverse matrix R_{qh}^{-1}. These elements are given by

$$R_{qh}^{-1}\ (11) = \left(1 - \frac{D}{f_x}\right)\left(1 - \frac{L_x}{f_h}\right) - \frac{D}{f_h} \tag{5.1a}$$

$$R_{qh}^{-1}\ (12) = - L_x \left(1 - \frac{D}{f_x}\right)\left(1 - \frac{D}{f_h}\right) + D \left(2 - \frac{D}{f_h} - \frac{D}{f_x}\right) \tag{5.1b}$$

$$R_{qh}^{-1}\ (21) = \frac{1}{f_h} + \frac{1}{f_x} - \frac{L_x}{f_h\ f_x} \tag{5.1c}$$

$$R_{qh}^{-1}\ (22) = \left(1 - \frac{D}{f_h}\right)\left(1 - \frac{L_x}{f_x}\right) - \frac{D}{f_x} \tag{5.1d}$$

If x_4 and x_4' are the horizontal displacement and slope at the entrance to the VC, the condition $x' = o$ at the exit of the HC is satisfied if focal length f_x satisfies the relation

$$-\frac{1}{f_x} = \frac{x_4 + x_4' \left(f_h - L_x\right)}{x_4 \left(f_h - L_x\right) - x_4' \left(f_h D + f_h L_x - L_x D\right)} \tag{5.2}$$

A smoothly varying tune for the four preconditioned sections is found by chosing $L_x = 3$ m and $Q_h = 1.15$ kG-m/m for $-10^o < \alpha_v < 10^o$. The quantities Q_v, Q_h, Q_x, θ_v and θ_h are plotted vs. α_v in Fig. 24 for $\alpha_h = 30^o$ and dp/p = 1%. The tune variations in Fig. 24 are still not ideal because of the discontinuity in the derivatives $\partial\theta_h/\partial\alpha_v$ and $\partial Q_h/\partial\alpha_v$.

We have not performed an extensive study of the effects of perturbations in magnet settings on the chromaticity of the system. For $\alpha_h = 30^o$ and

$\alpha_v = 20^\circ$ and $dp/p = 1\%$, calculations performed with the TRANSPORT code show that the system is achromatic in both planes to within 10 μrad and 0.1 mm if the setting of any one magnet in the preconditioner is accurate to within one part in 10^4. Clearly second order effects must be included before a meaningful study of tuning errors can be performed.

TABLE 1

$\alpha_h, \alpha_v = 30.\ , 20.$

$$m_S^{-1} = \begin{pmatrix} 1.0000 & -1.1750 & & & .31485 \\ .11402 & .86603 & & & -.50000 \\ & & 1.0000 & -1.1980 & .211243 \\ & & .05034 & .93969 & -.34202 \\ & & & & 1. \end{pmatrix} \begin{pmatrix} 0 \\ 0 \\ 0 \\ 0 \\ 1. \end{pmatrix}_1 = \begin{pmatrix} .31485 \\ -.50000 \\ .21124 \\ -.34202 \\ 1. \end{pmatrix}_2$$

$B_v = -1.94150$ kG

$$m_{Q_v}^{-1} = \begin{pmatrix} 1.2881 & -.57204 & & & 0 \\ -1.1526 & 1.2881 & & & 0 \\ & & .71186 & -.42796 & 0 \\ & & 1.1526 & .71186 & 0 \\ & & & & 1. \end{pmatrix} \begin{pmatrix} .31485 \\ -.50000 \\ .21124 \\ -.34202 \\ 1. \end{pmatrix}_2 = \begin{pmatrix} .69158 \\ -1.0069 \\ .29674 \\ 0 \\ 1. \end{pmatrix}_3$$

$\vartheta_v = -29.918082$

$$m_{\vartheta_v}^{-1} = \begin{pmatrix} -1.8041 & .92957 & & & 0 \\ .30623 & -.71208 & & & 0 \\ & & 1. & -4.8252 & -.29676 \\ & & 0 & 1. & 0 \\ & & & & 1. \end{pmatrix} \begin{pmatrix} .69158 \\ -1.0069 \\ .29674 \\ 0 \\ 1 \end{pmatrix}_3 = \begin{pmatrix} -2.18366 \\ .92877 \\ 0 \\ 0 \\ 1 \end{pmatrix}_4$$

$B_h = 0.6476225$ kG

$$m_{Q_h}^{-1} = \begin{pmatrix} .90389 & -.47597 & & & 0 \\ .38446 & .90389 & & & 0 \\ & & 1.0961 & -.52403 & 0 \\ & & -.38446 & 1.0961 & 0 \\ & & & & 1. \end{pmatrix} \begin{pmatrix} -2.18366 \\ .92877 \\ 0 \\ 0 \\ 1 \end{pmatrix}_4 = \begin{pmatrix} -2.4158 \\ 0 \\ 0 \\ 0 \\ 1 \end{pmatrix}_5$$

$\vartheta_h = 46.86321$

$$m_{\vartheta_h}^{-1} = \begin{pmatrix} 1. & -11.057 & & & 2.41593 \\ 0 & 1. & & & 0 \\ & & .64198 & .69597 & 0 \\ & & -.79989 & .69171 & 0 \\ & & & & 1. \end{pmatrix} \begin{pmatrix} -2.4158 \\ 0 \\ 0 \\ 0 \\ 1 \end{pmatrix}_5 = \begin{pmatrix} 0 \\ 0 \\ 0 \\ 0 \\ 1 \end{pmatrix}_6$$

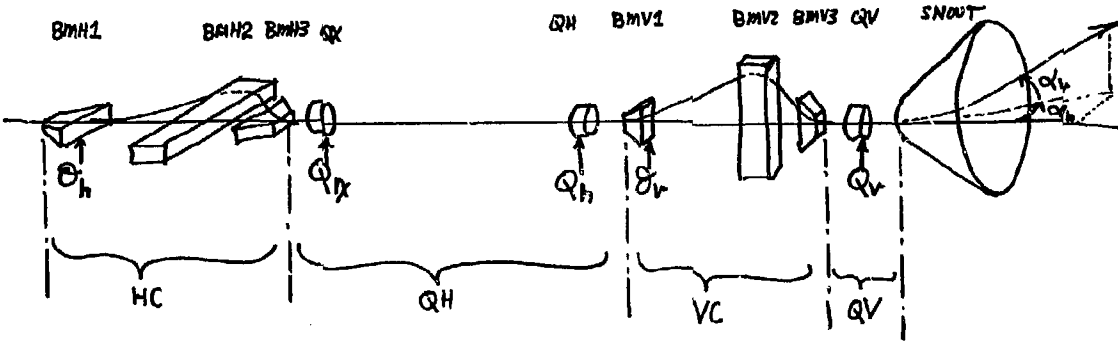

FIGURE 1. The double achromatic beam deflection system giving the designation of the sections and the names of individual magnets of the system.

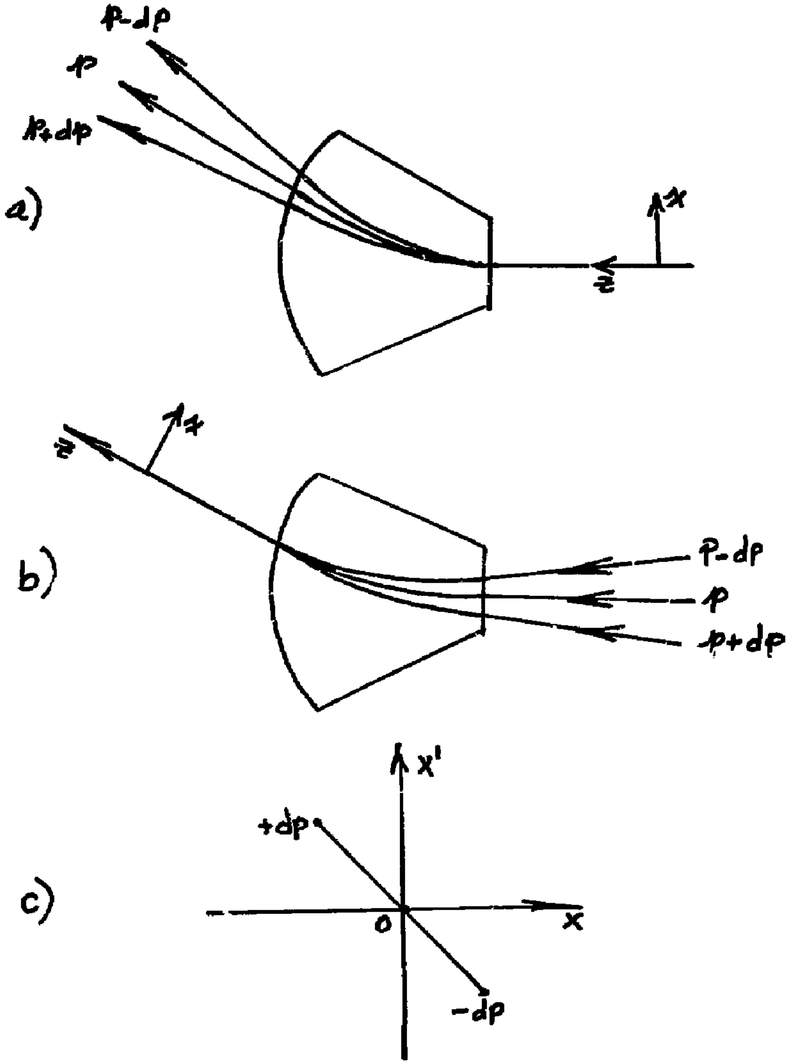

FIGURE 2. Dispersion in final bending magnet. a) Dispersion if beam is not preconditioned. b) Dispersion eliminated by proper preconditioning. c) Phase space is required at entrance to final bending magnet.

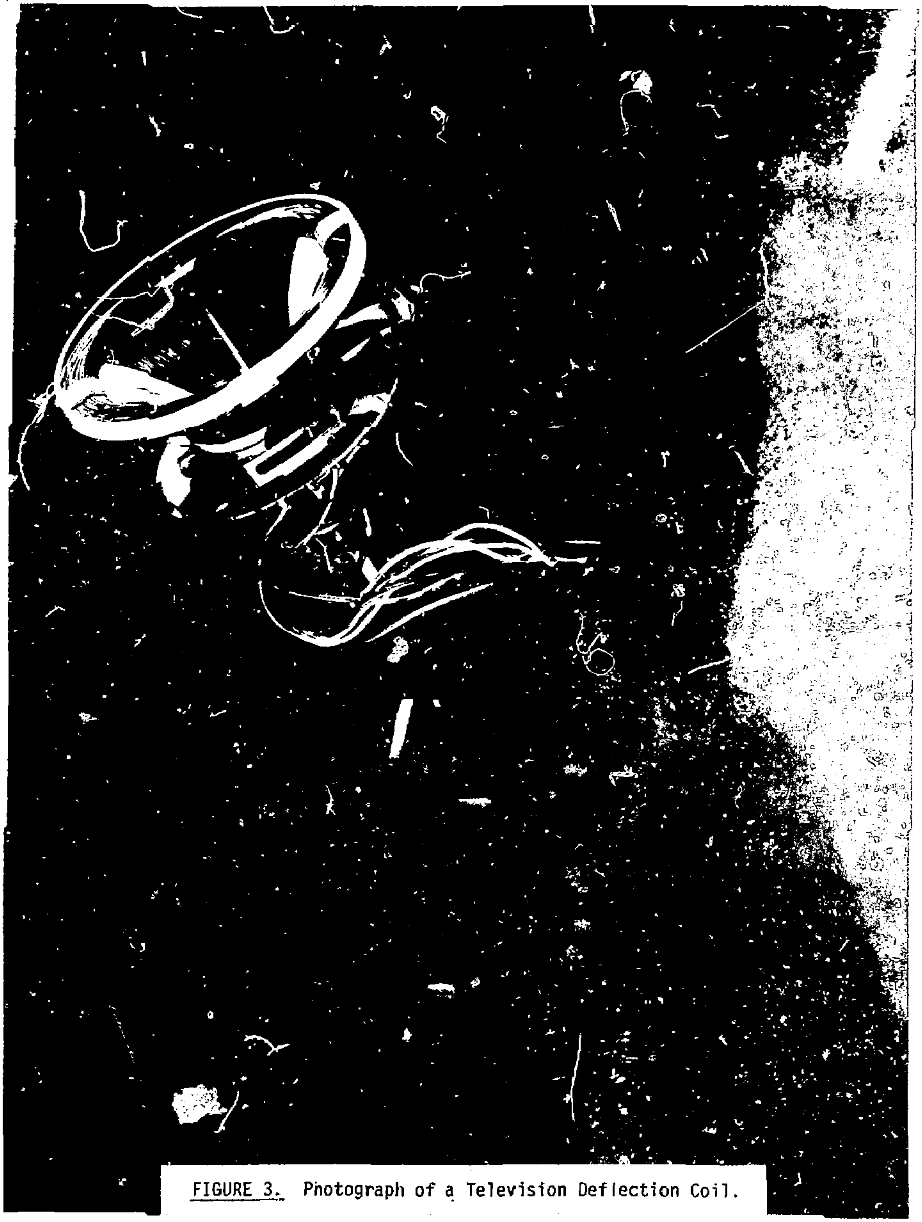

FIGURE 3. Photograph of a Television Deflection Coil.

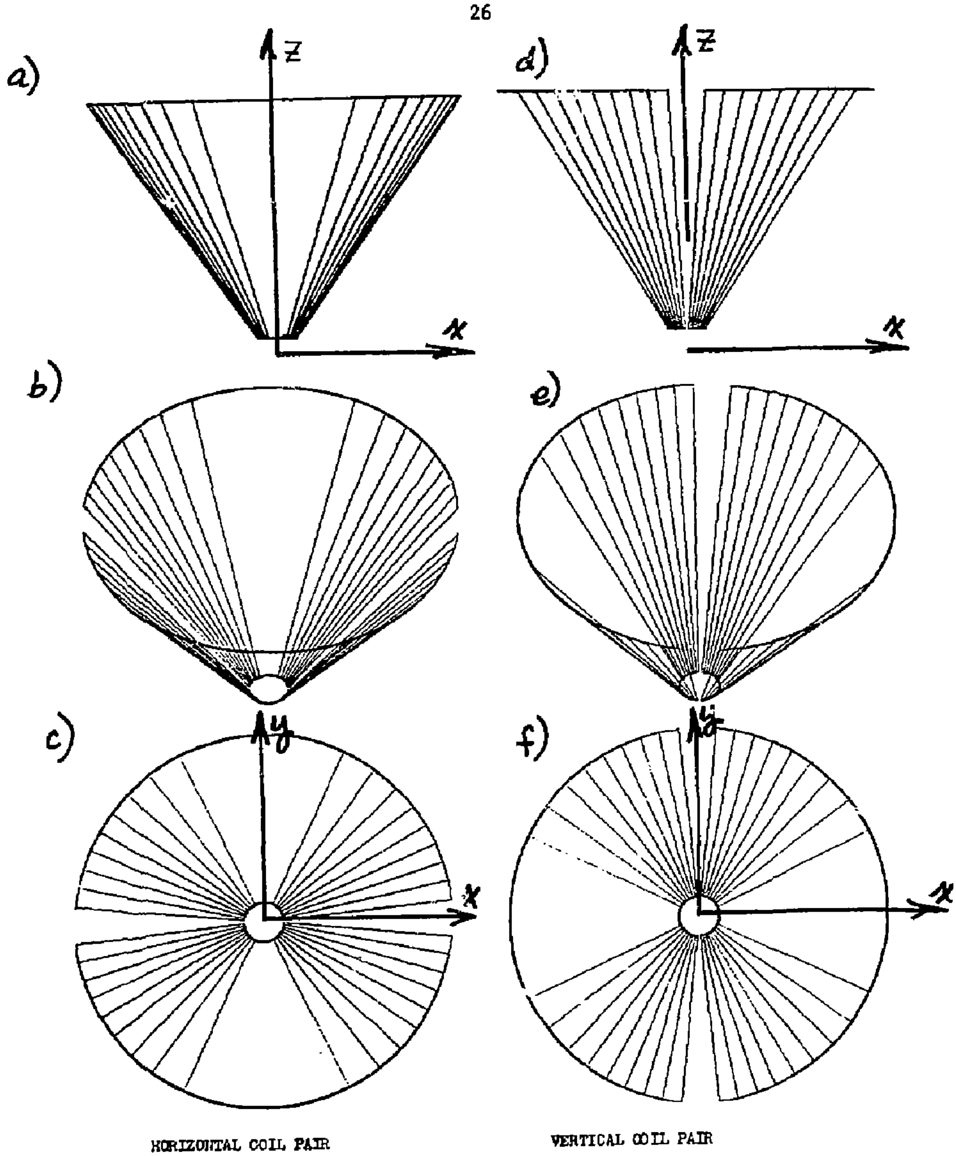

FIGURE 4. Coil windings employed 'n physical model of the deflection coil a), b), c) windings for deflection in x plane. d), e), f) windings for deflection in y plane.

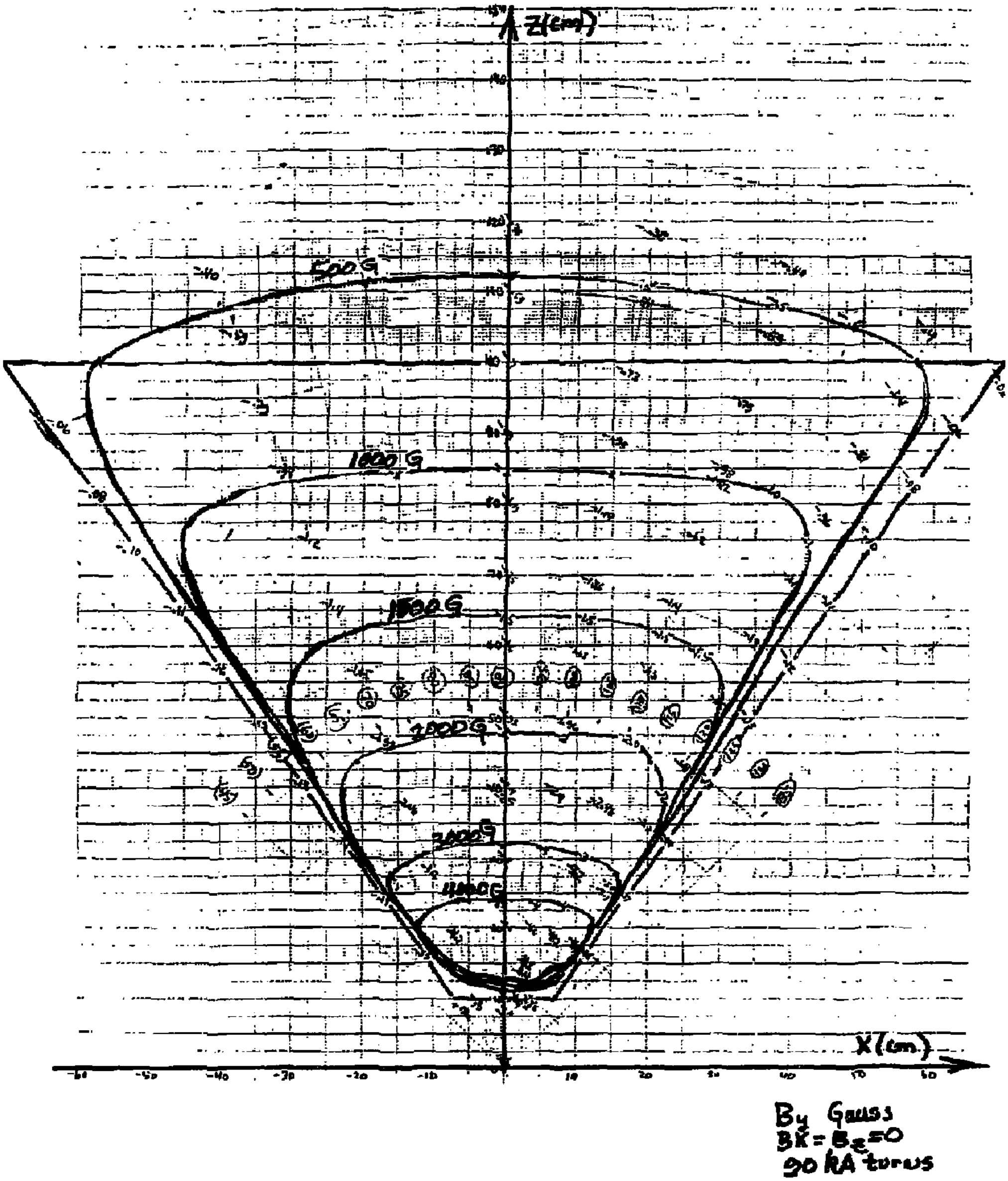

FIGURE 5. Contours of constant B_y in the plane y=0 generated by 90 kA-turns in the coil shown in figures 4 a,b, or c. The field values are in Gauss.

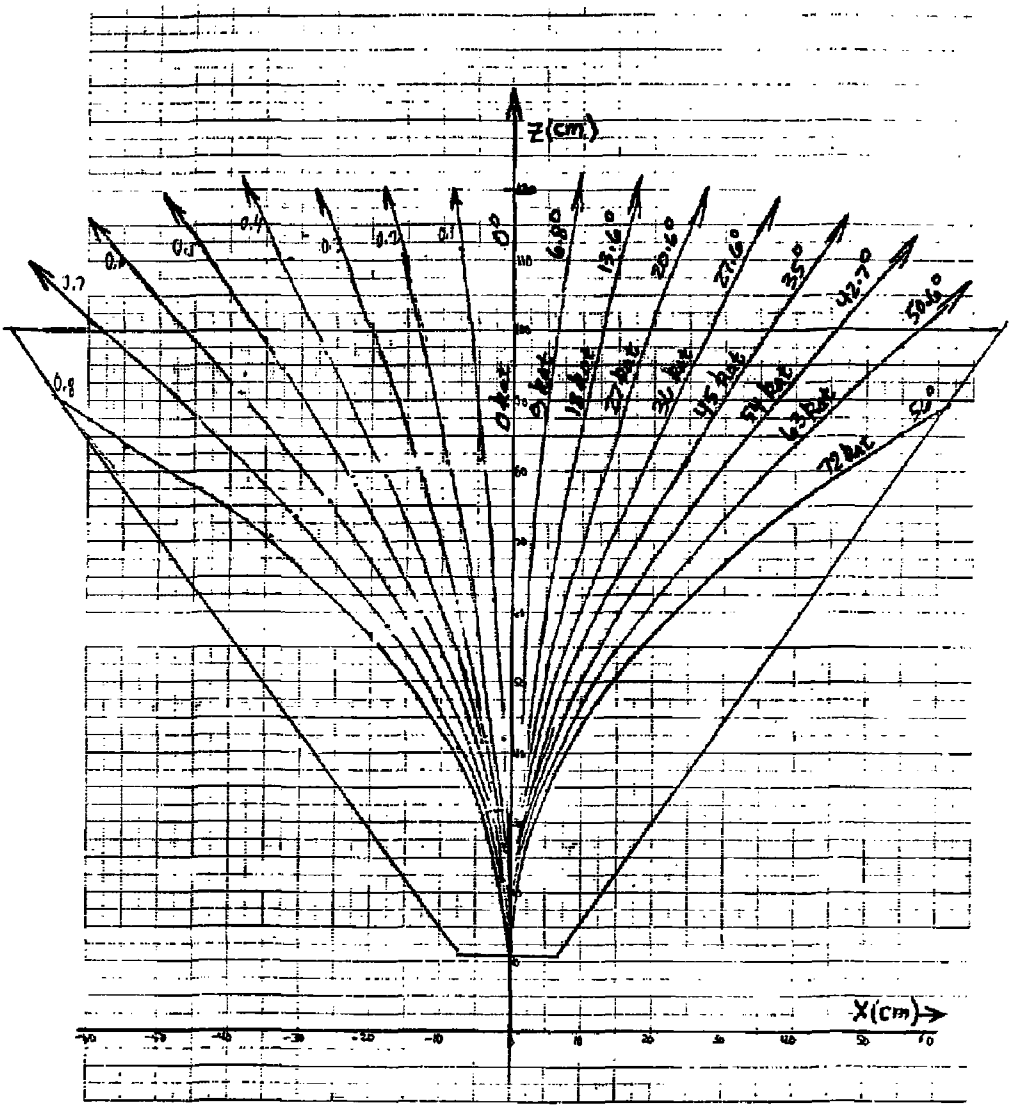

FIGURE 6. Trajectories of electrons with momentum p=50.5 MeV/C in the y=0 plane of the physical model. The Ampere turns per coil (fig. 4) required to achieve a given bending angle is also indicated.

FIGURE 7.

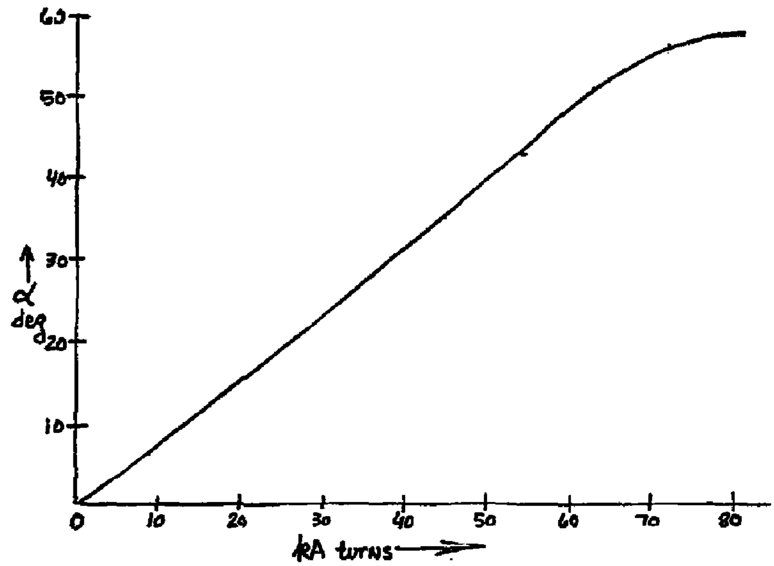

FIGURE 8.

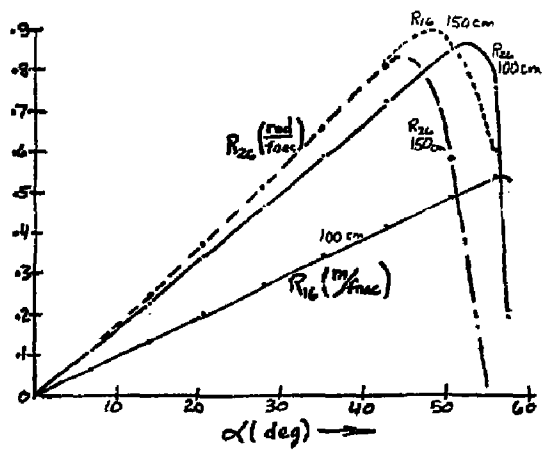

FIGURE 7. Bending angle α vs. required Ampere turns/coil in the physical model.

FIGURE 8. Dispersive matrix elements R_{16} and R_{26} vs. the bending angle in the physical model obtained by integrating particle trajectories.

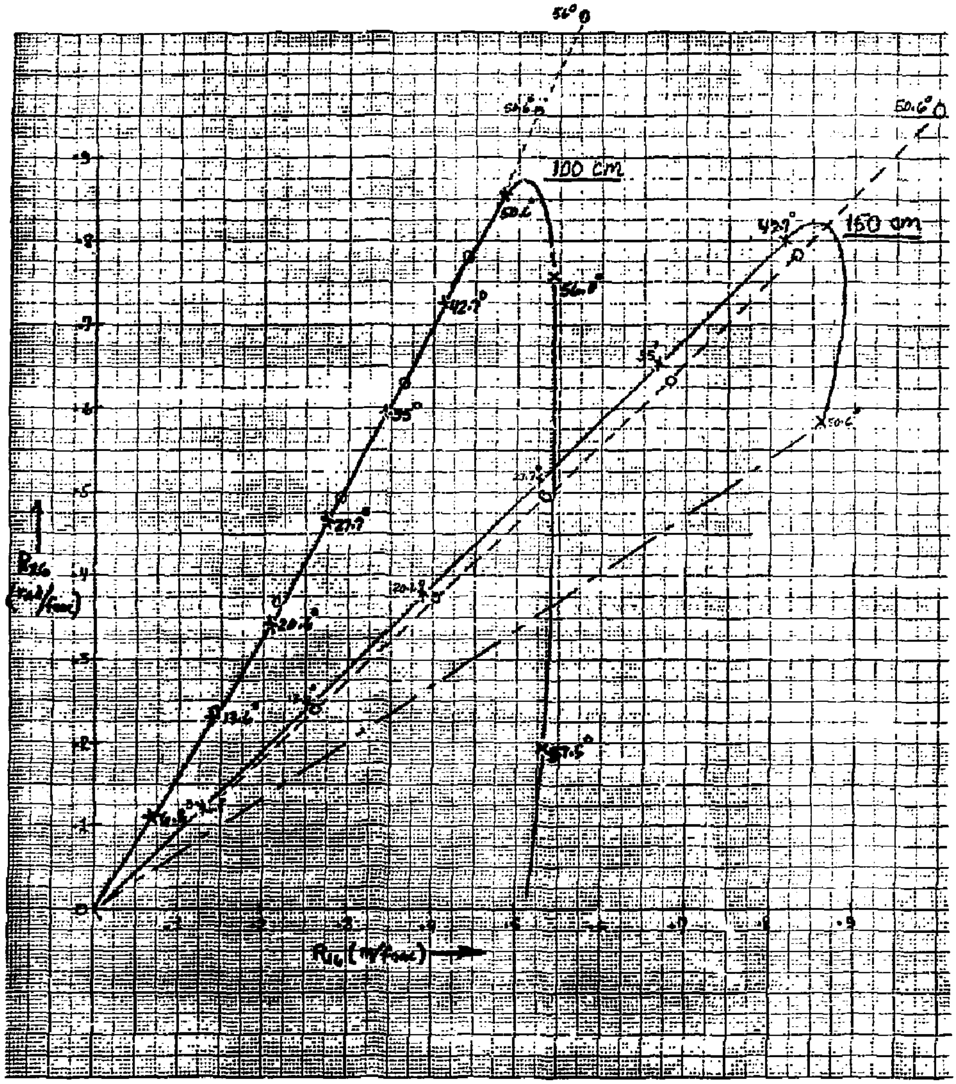

FIGURE 9. Dispersion curves of the physical (x) and analytic (o) models of the final deflection magnet for path lengths of 1.0 and 1.5 m.

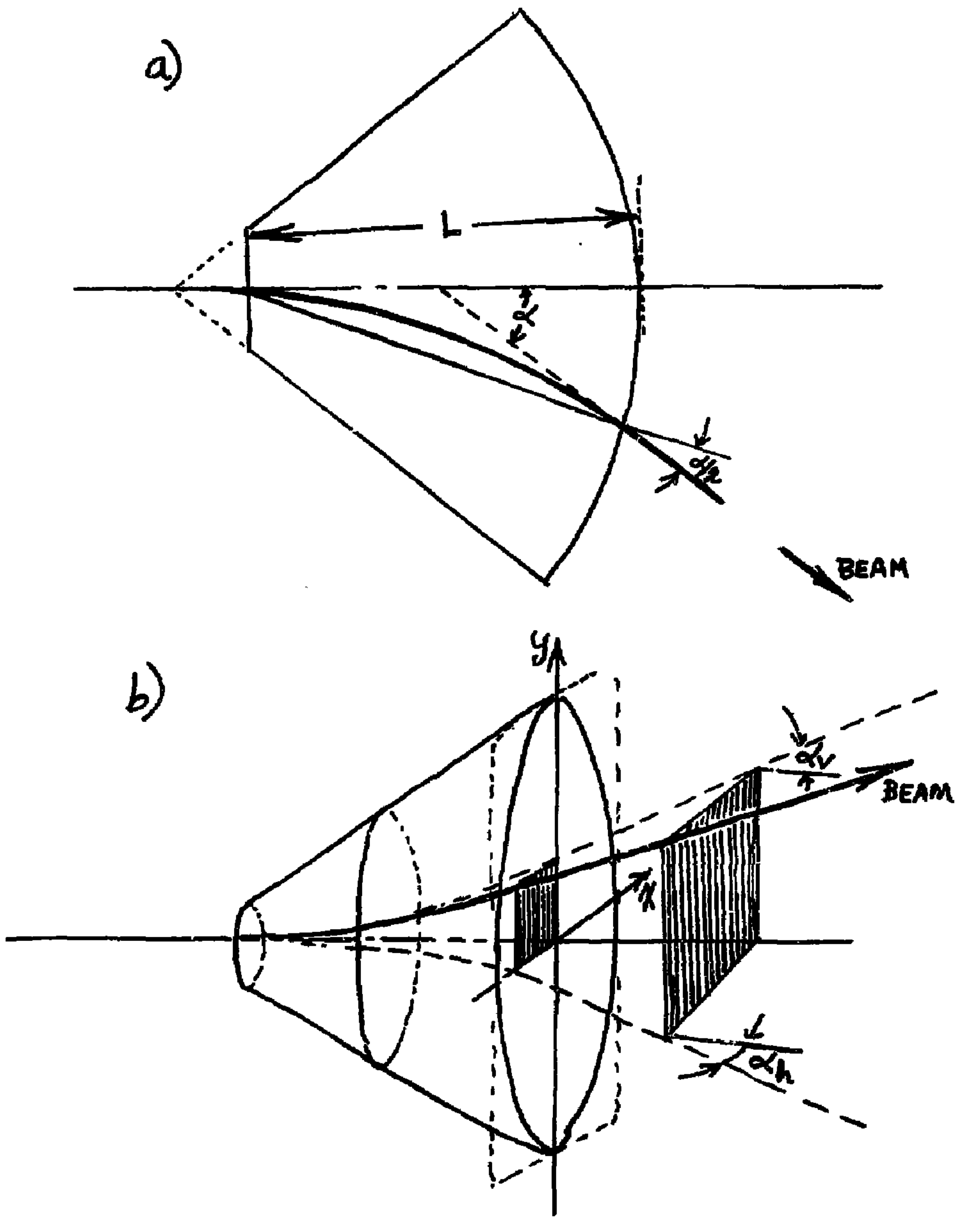

FIGURE 10. Schematic of particle trajectories in the final deflection magnet. a) analytic model, b) physical model.

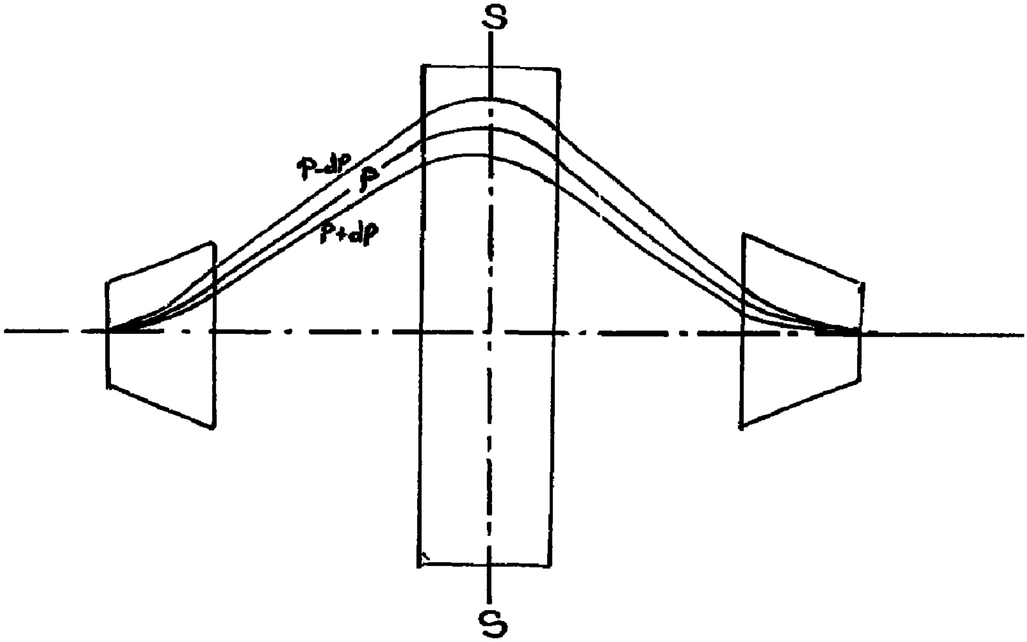

FIGURE 11. Symmetric three-dipole magnet array. Trajectories of particles with different momenta are recombined on exit so that the array is double achromatic in the bend plane.

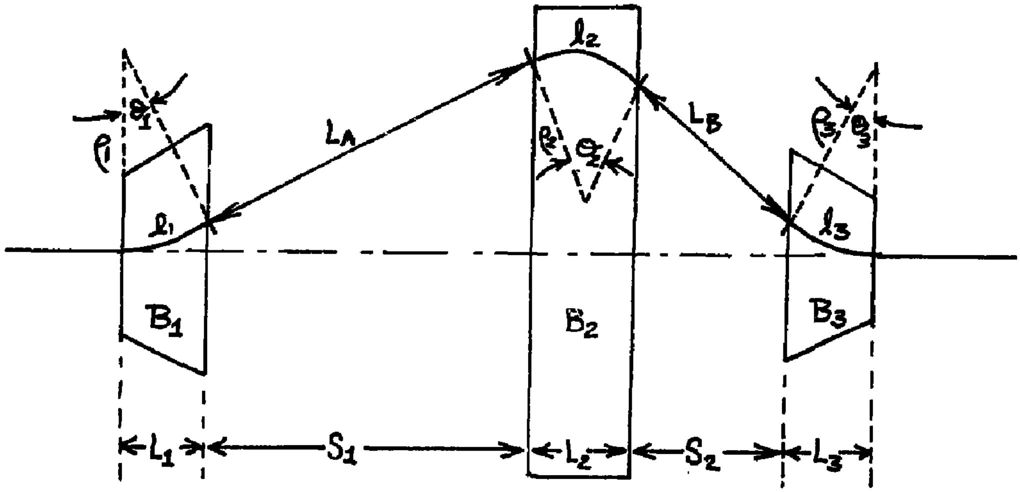

FIGURE 12. Asymmetric three-dipole magnet array with colinear trajectory. The path lengths are those of the reference particle.

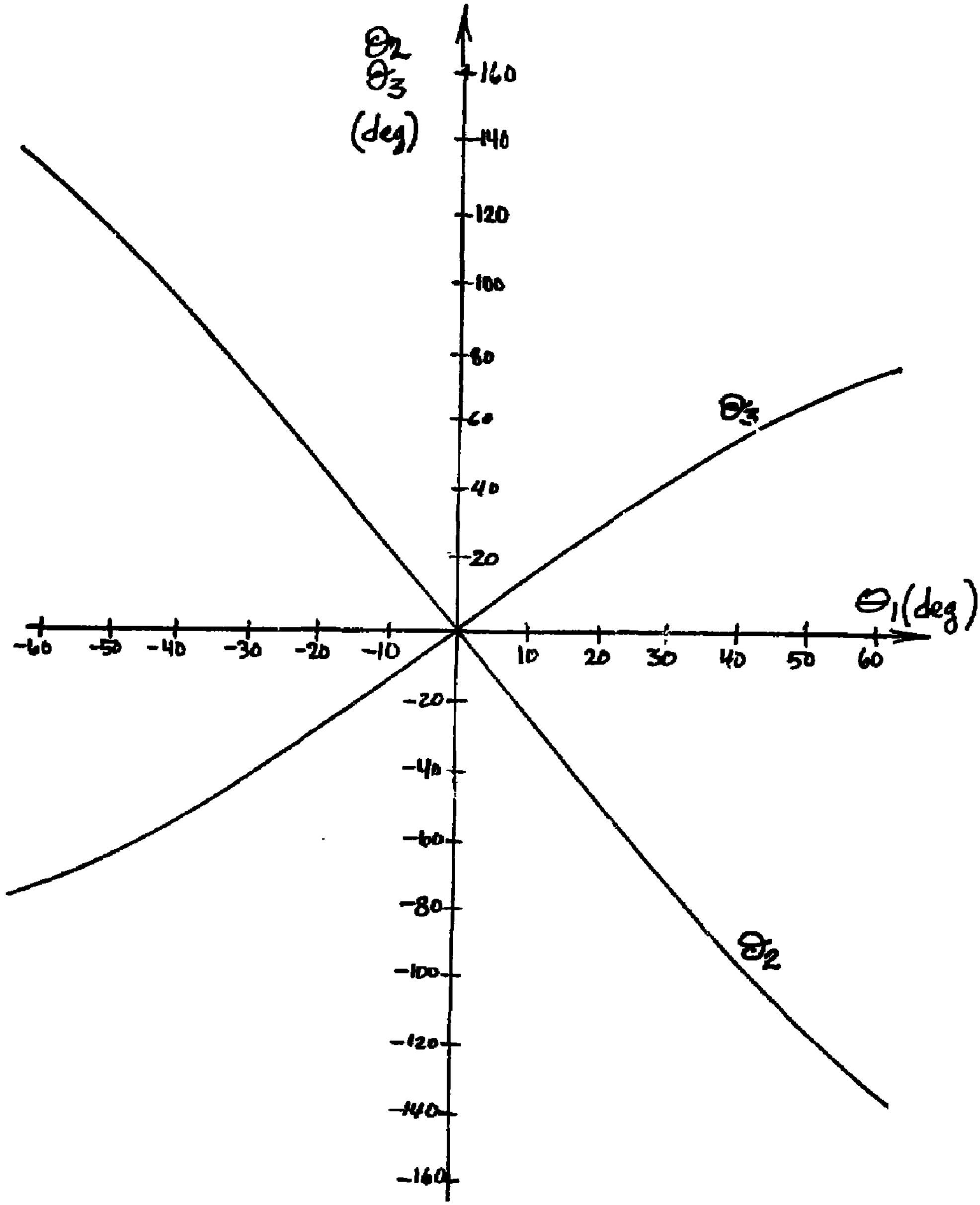

FIGURE 13. The angles θ_2 and θ_3 that are the solutions to Eqs. (3.1) and (3.2), required to produce a colinear reference trajectory in the three-dipole asymmetric array, Fig. 12.

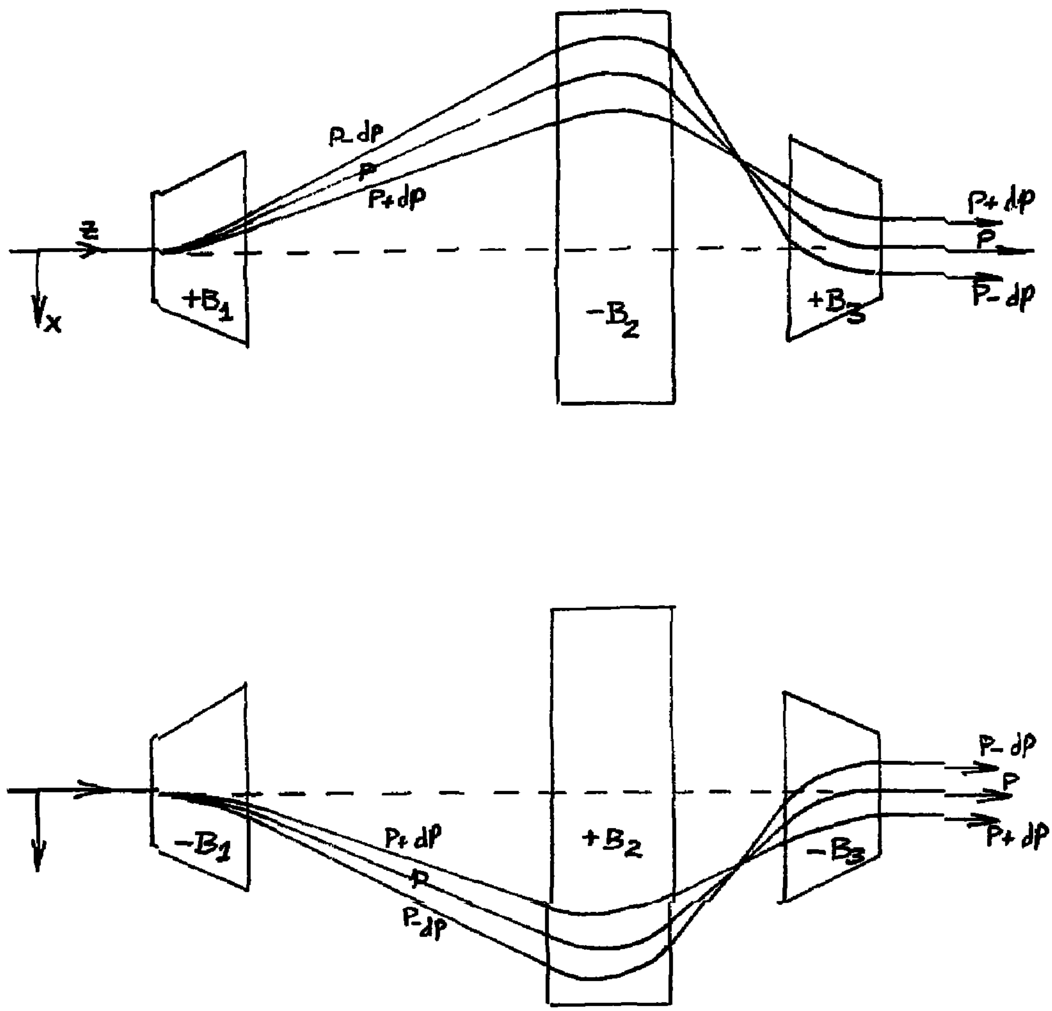

FIGURE 14. Trajectories of particles with different momenta in the three dipole array of Figure 12. The beam exits the array with no angular dispersion. There is a momentum focus between the second and third magnets.

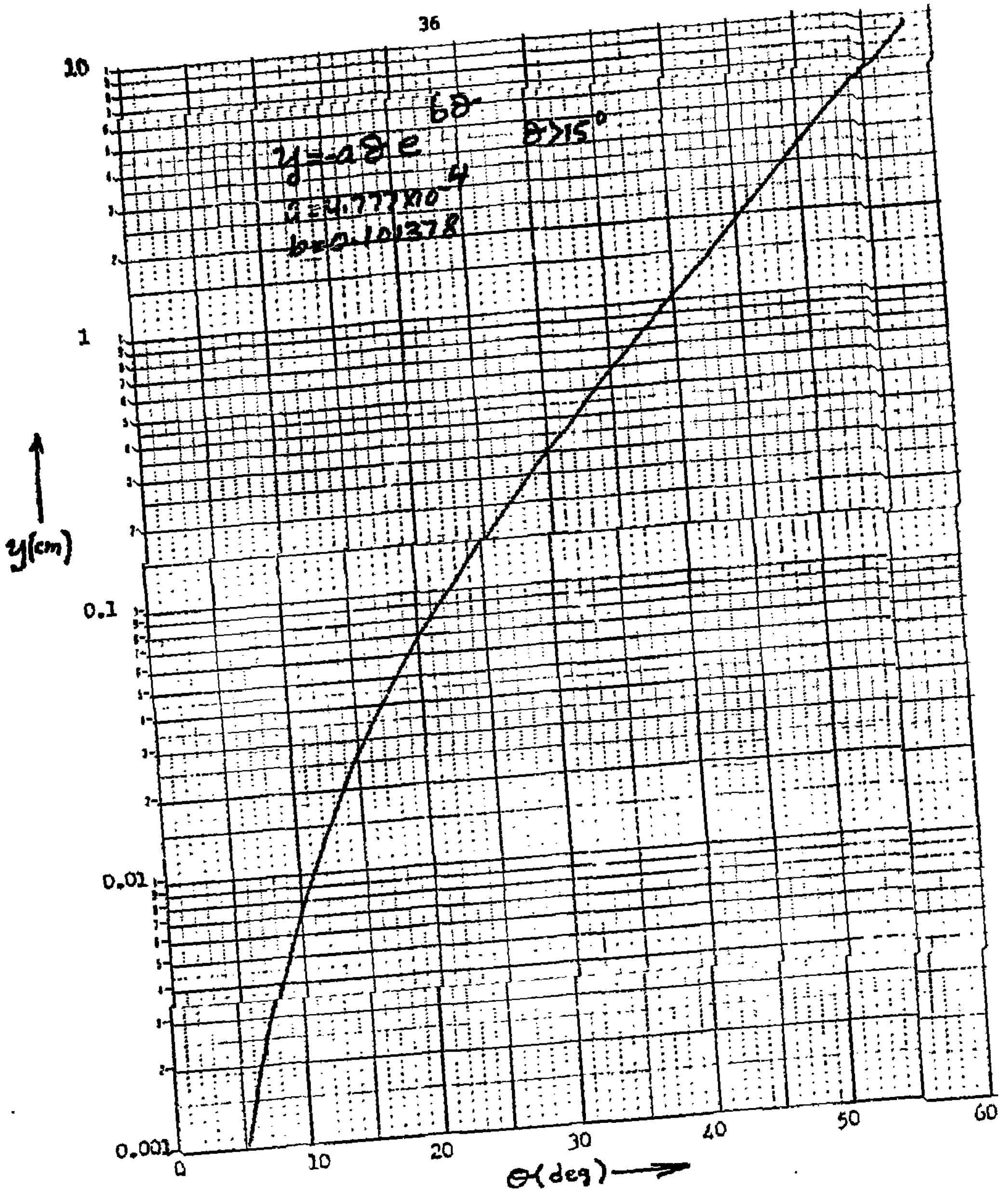

FIGURE 15. Positional dispersion vs. the angle θ_1 introduced by the magnet array of figures 12 and 14.

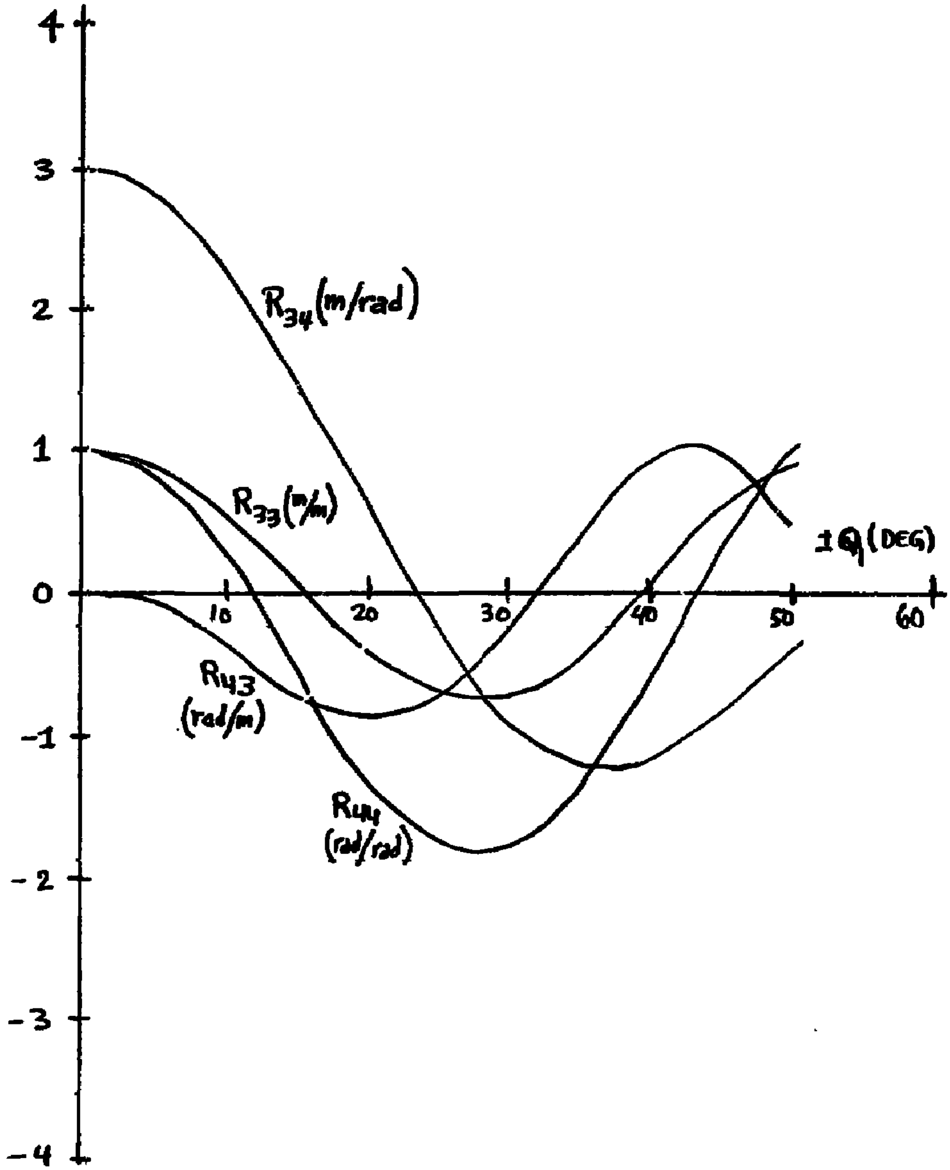

FIGURE 16. Matrix elements of the magnet array of figure 12 for the non-bend plane vs. the angle θ_1.

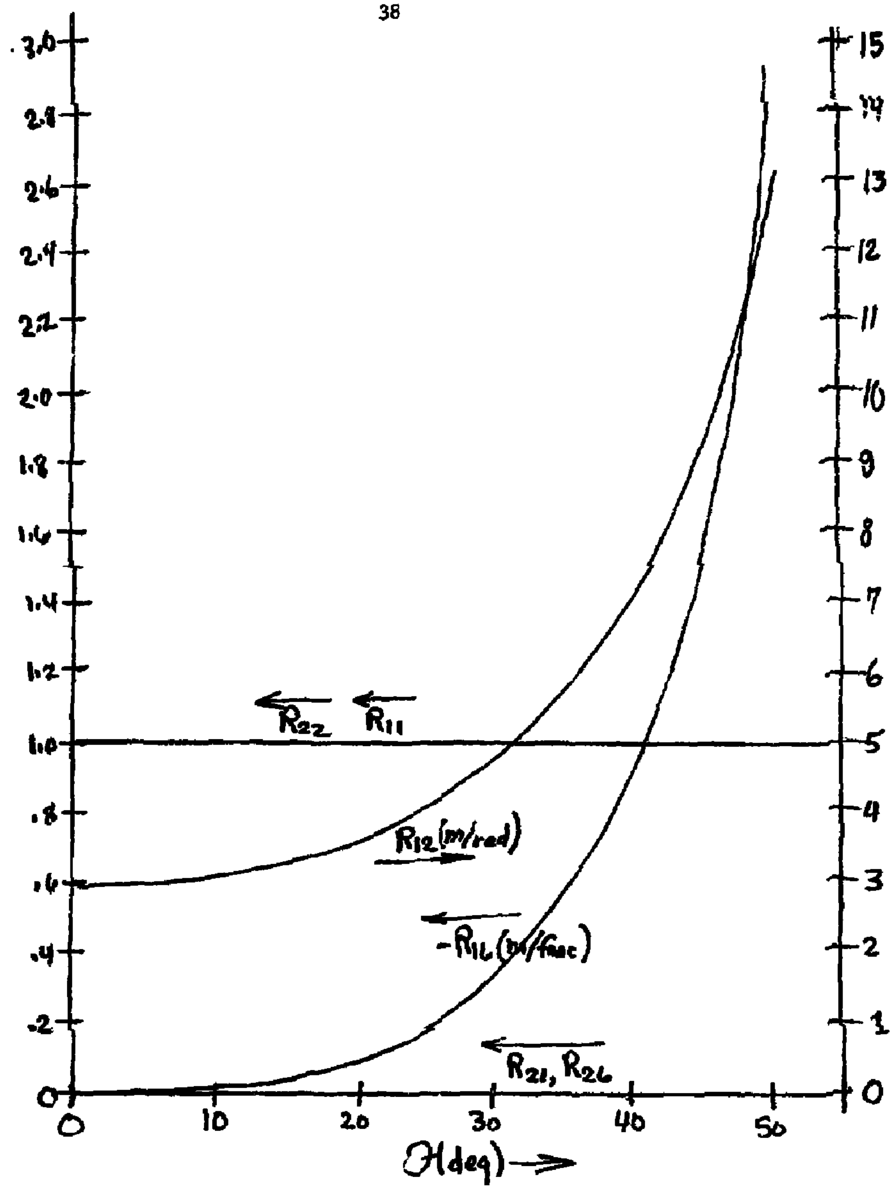

FIGURE 17. Matrix elements of the magnet array of Figure 12 for the bend plane vs. the angle θ_1. The array appears as a pseudo-drift space in this plane.

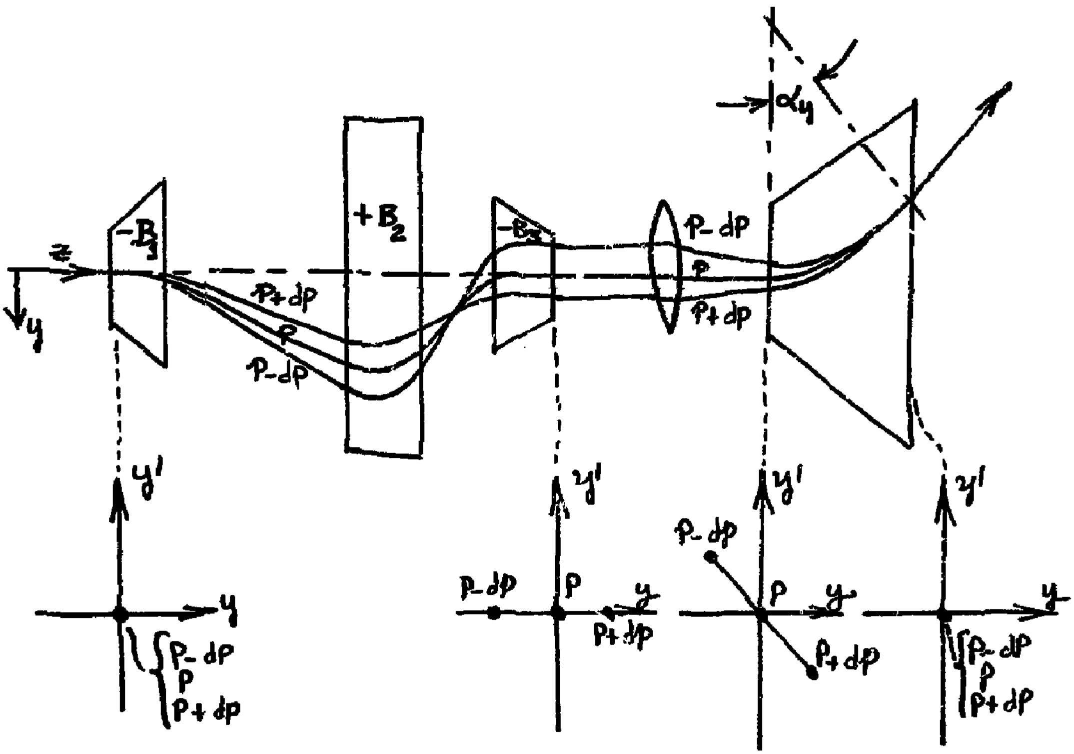

FIGURE 18. Vertical corrector, vertical quadrupole and snout showing preconditioned trajectories in the vertical plane and vertical phase space at various positions along the reference trajectory.

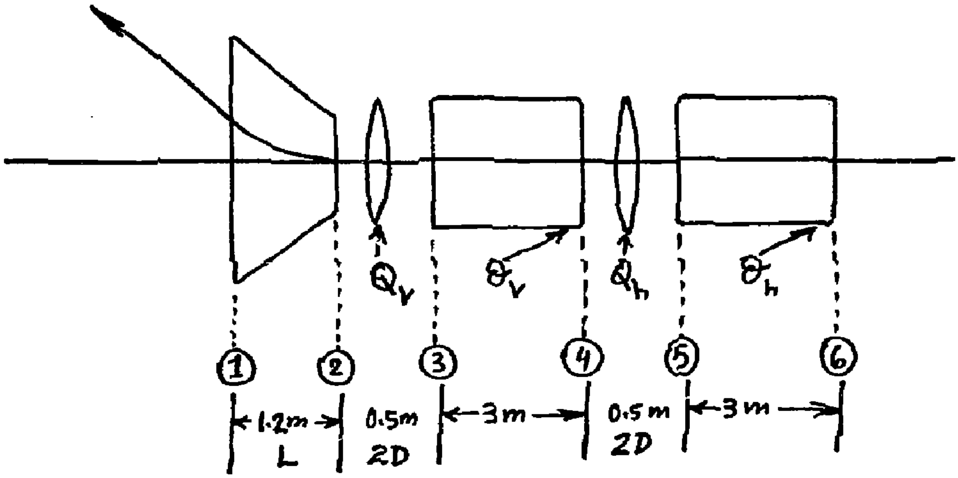

FIGURE 19. Schematic of snout magnet and four sections of the beam preconditioner as used in the numerical example, Table 1.

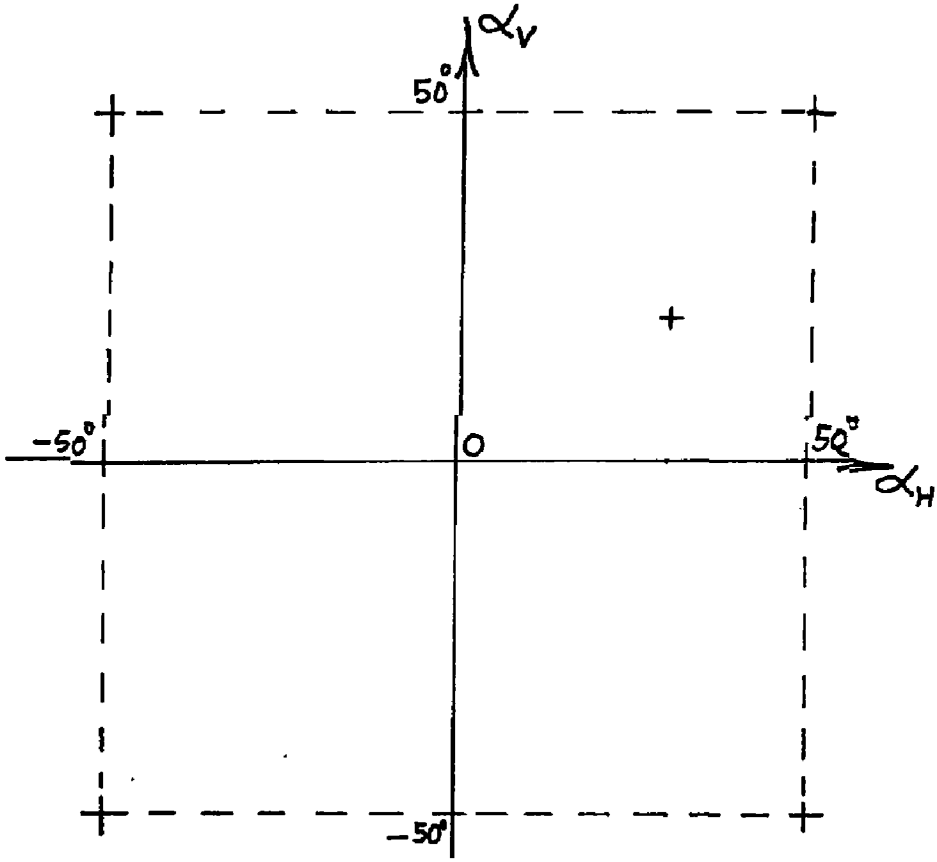

FIGURE 20. Snout deflection space showing a possible beam exit point.

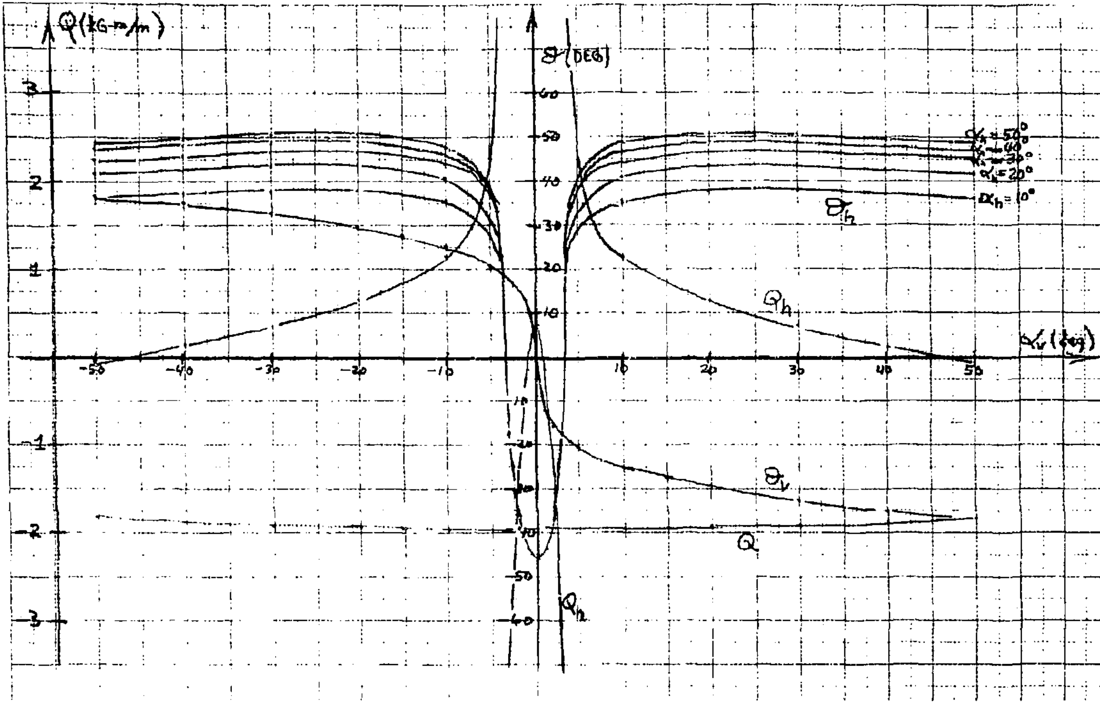

FIGURE 21. System tune vs. vertical bending angle α_v for the system shown in Figure 19. The values of Q_v and Q_h are in kG-m/m. Only θ_h varies significantly with horizontal bending angle α_h. Note the singularity in the Q_h and rapid change of θ_h near $|\alpha_v|$ of about 4 degrees.

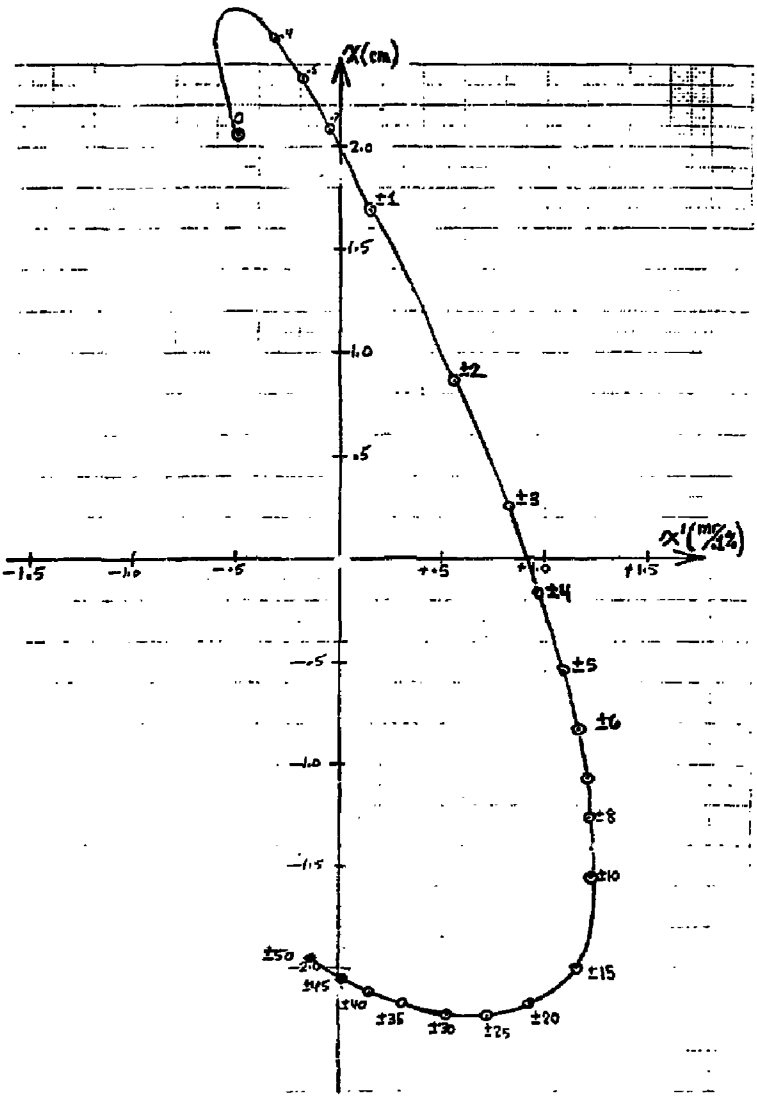

FIGURE 22. Plot of x and x' at the entrance to the vertical corrector as α_y is varied. Note that x passes through zero near α_y of 4 degrees.

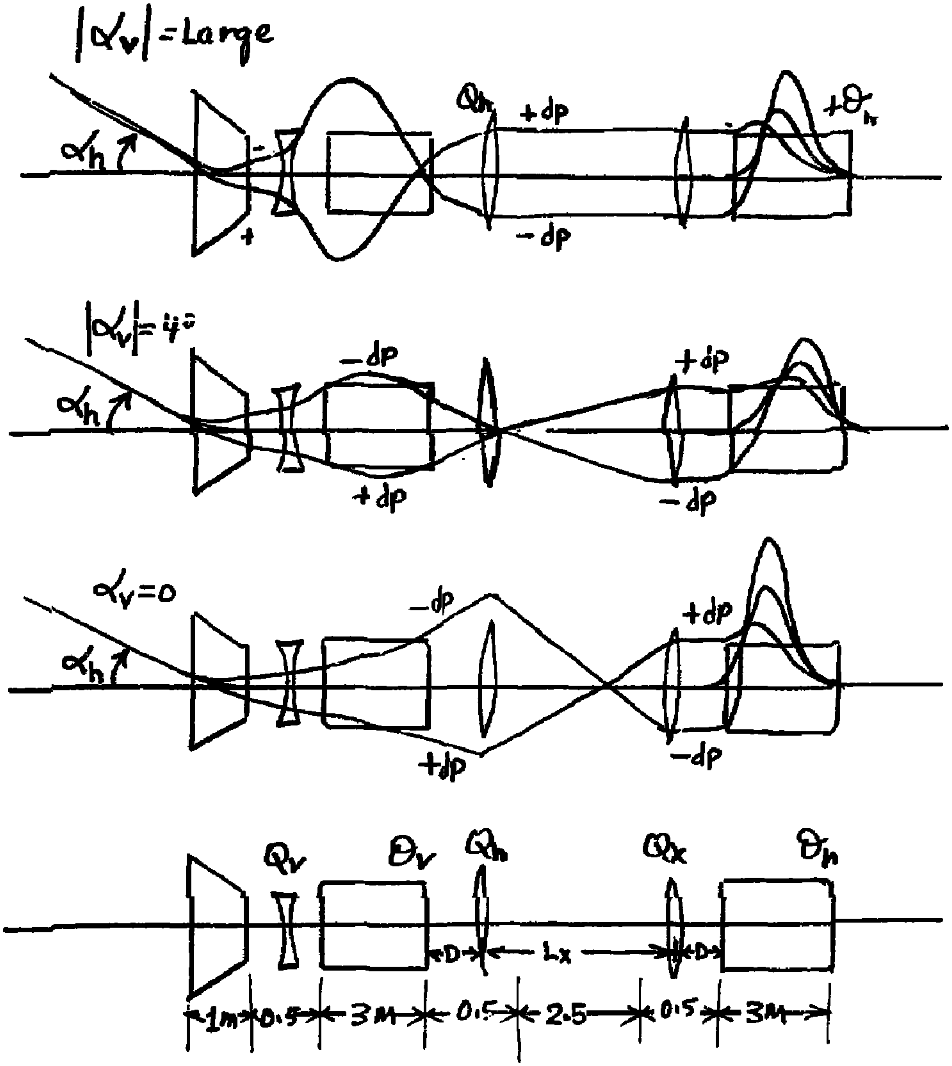

FIGURE 23. System with quadrupole Q_x added to the horizontal quadrupole section. The trajectories in the horizontal plane of particles with p±dp are shown qualitatively for various values of α_v.

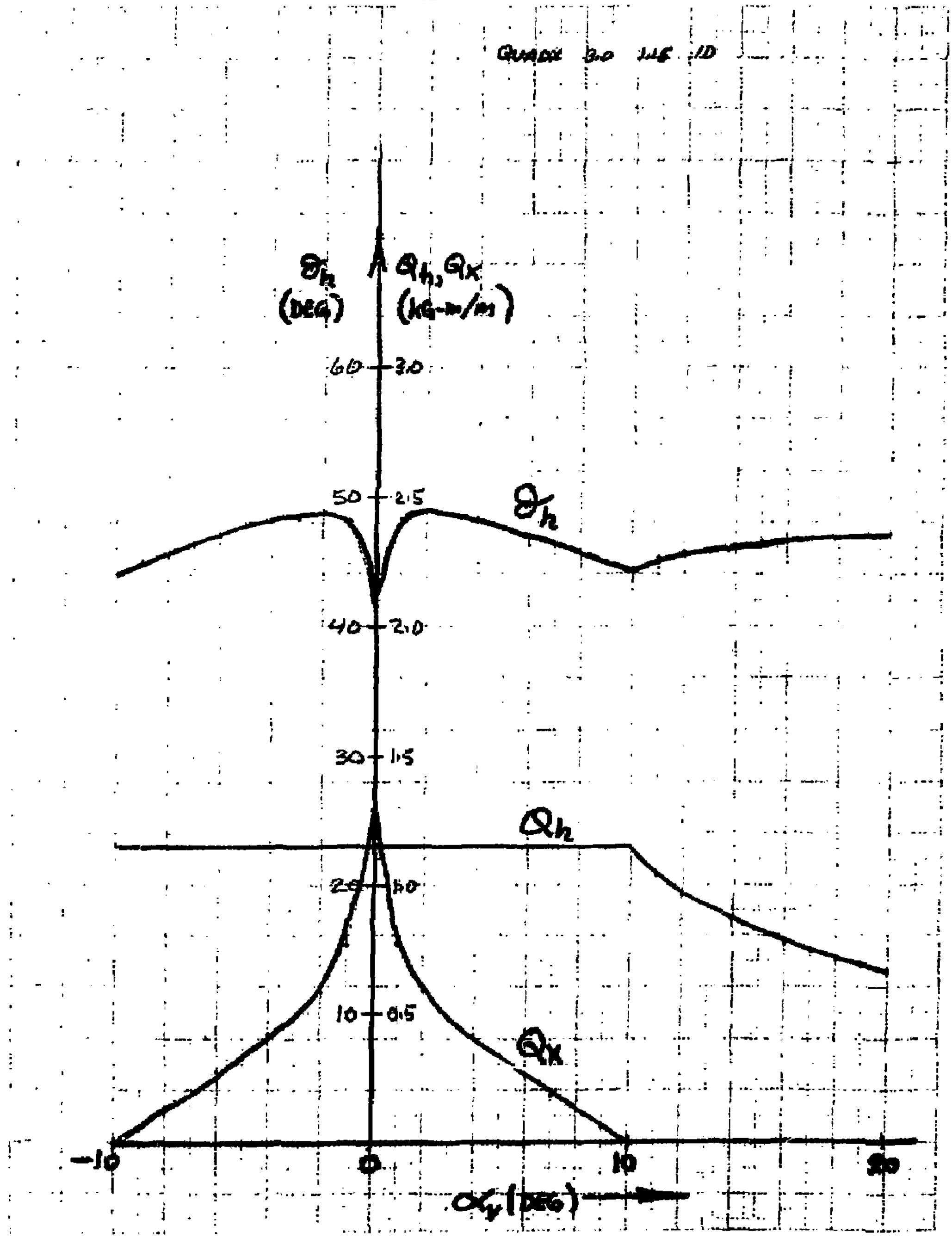

FIGURE 24. Tune of the horizontal preconditioner sections vs. α_v for $\alpha_h = 30^0$. The presence of the quadrupole Q_x removes the singularity at $|\alpha_v| \approx 4^0$.

Figure Captions

1. The doubly achromatic beam deflection systems giving the designation of the sections and the individual magnet.
2. Dispersion in final bending magnet. a) Dispersion if beam is not preconditioned. b) Dispersion eliminated by proper preconditioning. c) Phase space at required at entrance to final bending magnet.
3. Photograph of a Television Deflection Coil.
4. Coil windings employed in physical model of the deflection coil. a), b), c) Windings for deflection in x plane. d), e), f) Windings for deflection in y planes.
5. Contours of constant B_y in the plane y = o generated by 10,000 A in the coil shown in Fig. 4 a,b,c. The values are in Gauss.
6. Trajectories of electrons with momentum p = 50 MeV/c in the y = o plane of the physical model. The values of current are those in the 9-turn coil, Fig. 4 a,b,c, required to achieve a given bending angle.
7. Bending angle α vs. required current in the physical model.
8. Dispersive matrix elements R_{16} and R_{26} vs. bending angle in the physical model obtained by integrating particle trajectories over 1 m (solid curve) and 1.5 m (dashed curve).
9. Dispersion curves of the physical and analytic models of the final deflection magnet.
10. Schematic of particle trajectories in the final deflection magent. a) Analytic model, b) physical model.
11. Symmetric three-dipole magnet array. Trajectories of particles with different momenta are recombined on exit so that the array is doubly achromatic in the bend plane.

12. Asymmetric three-dipole magnet array with colinear trajectory. The path lengths are those of the reference particle.
13. The angles θ_2 and θ_3 that are solutions to Eqs. (3.1) and (3.2).
14. Trajectories of particles with different momenta in the three dipole array in Fig. 13. The beam exits the array with no angular dispersion. There is a momentum focus between the second and third magnets.
15. Positional dispersion vs. the angle θ_1 introduced by the magnet array in Fig. 13.
16. Matrix elements of the magnet array in Fig. 13 for the non-bend plane vs. the angle θ_1.
17. Matrix elements of the magent array in Fig. 13 for the bend plane vs. the angle θ_1. The array appears as a drift space in this plane.
18. Vertical connector, vertical quadrupole and snout showing preconditioned trajectories in the vertical plane and vertical phase space at various positions.
19. Schematic of snout magnet and four sections of the preconditioner as used in the numerical example, Table 1.
20. Four squares and some dots.
21. System tune vs. vertical bending angle α_v for the system shown in Fig. 19. The values of Q_v and Q_h are in kG-m/m. Only θ_h varies significantly with horizontal bending angle α_h. Note the singularity in Q_h and rapid change of θ_h near $|\alpha_v| = 4^{\circ}$.
22. Plot of x and x' at the entrance to the vertical corrector as α_v is varied. Note that x passes through zero near $\alpha_v = 4^{\circ}$.

23. System with quadrupole Q_x added tot he horizontal quadrupole section. The trajectories in the horizontal plane of particles with $p \pm dp$ are shown qualitatively for various values of α_v.

24. Tune of the horizontal preconditioner sections vs. α_v for $\alpha_h = 30^o$. The presence of the quadrupole Q_x removes the singularities at $|\alpha_v| \gtrsim 4^o$.

References

1. "TRANSPORT, An Ion Optic Program, LBL Version", Arthur C. Paul, Lawrence Berkeley Laboratory Report LBL-2697, (1975). This report contains references to many earlier publications.
2. "MAFCO - A Magnetic Field Code for Handling General Current Elements in three Dimensions" W.A. Perkins, J.C. Brown, Lawrence Livermore Laboratory report UCRL-7744 (1966).
3. "TRAJECTORY - An Orbit and Ion Optic Matrix Program for the 184-Inch Cyclotron" A.C. Paul, Lawrence Berkeley Laboratory report UCRL-19407, (1969).
4. "Recent Advance in Electron Beam Deflection", Edward F. Ritz, Jr., Advances in Electronics and Electron Physics, Vol. 49, (1979).